Fall 2014

Femtosecond laser micro-machined optical fiber based embeddable strain and temperature sensors for structural monitoring

Armadeep Kaur
Missouri University of Science and Technology, kaura@mst.edu

Department: Electrical and Computer Engineering

FEMTOSECOND LASER MICRO-MACHINED OPTICAL FIBER BASED EMBEDDABLE STRAIN AND TEMPERATURE SENSORS FOR STRUCTURAL MONITORING

by

AMARDEEP KAUR

A DISSERTATION

Presented to the Faculty of the Graduate School of the
MISSOURI UNIVERSITY OF SCIENCE AND TECHNOLOGY
In Partial Fulfillment of the Requirements for the Degree

DOCTOR OF PHILOSOPHY
in
ELECTRICAL ENGINEERING

2014

Approved by

Dr. Hai Xiao, Co-Advisor
Dr. Steve E. Watkins, Co-Advisor
Dr. Hai-Lung Tsai
Dr. Chang-Soo Kim
Dr. Randy H. Moss

ABSTRACT

Structural monitoring technology is becoming increasingly important for managing all types of structures. Embedding sensors while constructing new structures or repairing the old ones allows for continual monitoring of structural health thus giving an estimate of remaining utility. Along with being embeddable, miniaturized sensors that are easy to handle are highly sought after in the industry where in-situ monitoring is required in a harsh environment (corrosive atmosphere, high temperatures, high pressure etc.).

This dissertation demonstrates the use of femtosecond laser-fabricated Fabry-Perot interferometer (FPI) based optical fiber sensors for embedded applications like structural health monitoring. Two types of Fabry-Perot interferometer sensors, extrinsic FPI and intrinsic FPI, have been designed, developed and demonstrated for strain and temperature monitoring applications. The absence of any movable parts make these sensors easy-to-handle and easy to embed inside a material. These sensors were fabricated using a laboratory integrated femto-second (fs) laser micromachining system. For the extrinsic Fabry-Perot interferometer (EFPI) design, the fs-laser was used to ablate and remove the material off the fiber end face while for intrinsic Fabry-Perot interferometer (IFPI) design, the laser power was focused inside the fiber on the fiber core to create two microstructures. The scope of the work presented in this dissertation extends to device design, laser based sensor fabrication, sensor performance evaluation and demonstration.

Feasibility of using these sensors for embeddable applications was investigated. A new type of material called Bismaleimide (BMI) was used for demonstrating the embeddability of the sensors. Experimental results of strain and temperature testing are presented and discussed. The EFPI sensor has low temperature sensitivity of 0.59 pm/ºC and a high strain sensitivity of 1.5 pm/με. The IFPI sensor has the same strain sensitivity as EFPI but is 25 times more sensitive to the temperature. These sensors were tested up to 850 ºC in non-embedded condition and they produced a linear response. A hybrid approach combining the EFPI and IFPI sensors was demonstrated for simultaneous measurement of strain and temperature.

ACKNOWLEDGEMENTS

I thank my family, colleagues, mentors and numerous others who have contributed so much during my studies. I am very thankful to my family for understanding my commitments and lending their support these past years. My stay in Rolla would not have been as easy and successful without the support of my husband Raj Singh who with his own commitments made sure to give me all the time and encouragement that I demanded.

I am immensely grateful to my co-advisors Dr. Hai Xiao and Dr. Steve E. Watkins for their immense support, guidance and patience throughout my graduate years. I am also thankful to them for giving me this opportunity to pursue research under their guidance. I am also thankful to Dr. Hai-Lung Tsai, Dr. Chang-Soo Kim and Dr. Randy H. Moss for their guidance on my dissertation, serving on my committee and for their encouragement over last several years.

I also take this opportunity to thank my fellow graduate students Xinwei Lan, Lei Yuan, Jie Liu, Jie Huang, Yinan Zhang, Hanzheng Wang, Mujahid Abdul, Tameem Khan, Adviya Saba, Baokai Cheng, Dr. Qun Han and Dr. Tao Wei for always being there amd extending a helping hand during testing times.

This research would not have been possible without the support and contribution of Dr. K. Chandarashekhara's group. I am thankful to him and everybody associated with the Composites Manufacturing Laboratory at S&T for letting me use their laboratory facilities and thus producing valuable research. I am really thankful to Sudharshan Anandan and Sriram Nagarajan for their time, help and assistance.

Finally, I thank the sponsors for this project, the U.S. Department of Energy, for sponsoring this research through the National Energy Technology program.

TABLE OF CONTENTS

Page

LIST OF ILLUSTRATIONS

Page

LIST OF TABLES

Page

LIST OF ABBREVIATIONS/NOMENCLATURE

Symbol	Description
EMI	Electromagnetic Interference
EFPI	Extrinsic Fabry-Perot Interferometer
fs	Femtosecond
IFPI	Intrinsic Fabry-Perot Interferometer
BMI	Bismaleimide (Carbon reinforced polymer)
MEMS	Microelectromechanical systems
FBG	Fiber Bragg Grating
LPFG	Long Period Fiber Grating
OSA	Optical Spectrum Analyzer
$\mathcal{F}$	Finesse
CTE	Coefficient of thermal expansion
nm	Nanometer
μm	Micrometer
$\mu\varepsilon$	Micro strain
FFT	Fast Fourier Transform

1. INTRODUCTION

Repair and maintenance of civil, automotive, and mechanical structures are very important and the cost of maintaining infrastructure is significant. Recent years have seen a new development in the field namely embedded sensors as a smart structures technology. Embedding sensors while constructing a new structure or repairing the old ones allows for continual monitoring of structural health thus giving an estimate of remaining utility. Along with being embeddable, miniaturized sensors that are easy to handle are highly sought after in the industry where in-situ monitoring is required in harsh environments. These harsh environments may be due to corrosive atmosphere, high temperature, high pressure, and presence of strong electromagnetic interference (EMI) noise. Sensors currently available have limitations in meeting these conditions. This existing gap provides an opportunity for innovative research to fabricate and demonstrate new sensors.

Optical fiber sensors have gained wide interests in the field of structural health monitoring applications due to their compact size, immunity from electromagnetic interference, multiplexing capabilities, etc. These sensors can either be embedded inside a material or surface mounted to monitor the parameters like strain, temperature, stress etc. The data can be collected continuously and analyzed for any abnormalities or patterns that suggest potential structural weakening or failure thus providing an opportunity to take necessary steps in order to maintain the structural integrity.

This dissertation proposes the use of femtosecond laser-fabricated Fabry-Perot interferometer based optical fiber sensors for embedded applications like structural health monitoring. These micro-cavity based sensors are ideal for embeddable applications because the sensors only comprise of the optical fiber itself. These rugged sensors have excellent noise-free performance and fatigue characteristics. The absence of any movable parts make these sensors easy-to-handle and easy to embed inside a material. The low loss of the optical fiber over the long distances mean that the instrumentation collecting data of a structure can be housed off-site depending upon the nature of the application. To meet the objectives, two basic optical fiber sensor designs were explored that were

fabricated using a laboratory integrated femto-second laser micromachining system. For the extrinsic Fabry-Perot interferometer (EFPI) design, the fs-laser was used to ablate and remove the material off the fiber end face while for intrinsic Fabry-Perot interferometer (IFPI) design, the laser power was focused inside the fiber on the fiber core to create two microstructures.

These sensors were tested for their embeddability characteristics by embedding them inside carbon-reinforced fiber composite laminates known as Bismaleimide (BMI). This type of material is used in the structures where high flexibility in addition to strength is needed, e.g. airplane wings, turbine blades, windmill blades etc. The BMI samples with the embedded sensors were subjected to strain and high temperature conditions to monitor the sensor response. The extrinsic Fabry-Perot interferometer (EFPI) sensor is proposed for strain monitoring at high temperatures due to its low temperature sensitivity. The intrinsic Fabry-Perot interferometer (IFPI) is proposed for strain applications at room temperatures due to its high temperature sensitivity. The two sensors have the same strain sensitivity but different temperature sensitivities and thus, a sensor combining the EFPI and IFPI has also been demonstrated for simultaneous measurement of the strain and temperature. In this case, the EFPI component can be used to calibrate the strain and thus the temperature information can be extracted using the IFPI sensor response. The response of the sensors was measured by observing their reflection spectra.

The work is presented in different sections. Section 2 presents a literature review of the motivation behind the research work carried out, fabrication techniques in use for similar sensors, applications for the proposed sensors, etc. Fabrication and the operational principle of the sensors are described and discussed in section 3 followed by the experiments set up and results that are discussed in Section 4. Section 5 offers an insight into the proposed sensor for simultaneous measurement of temperature and strain. Experiments conducted and data processing techniques have been discussed and explained in this section. Section 6 is used to summarize the presented work. Recommendations for future work that can be built upon the presented research have also been provided in this section.

2. LITERATURE REVIEW

This section presents a general introduction to optical fiber sensors with an emphasis on manipulating the optical fiber properties to use them for structural health monitoring and high temperature applications (specifically high temperature). A brief review of the current technologies available, challenges of using them and their limitations is provided followed by the motivation and objectives of this dissertation. The contributions and novel innovations presented in this work are also listed.

2.1 BACKGROUND

Since the conception of the optical fibers as a medium of transmitting light and imagery to being used in the telecommunication applications, the field of optical fiber applications has widened immensely [1][2]. The optical fiber sensors have been used in wide range of applications including structural health monitoring, biological sensors, medical imaging etc. These sensors are generally fabricated by manipulating the physical properties of the optical fiber.

Figure 2.1 shows the waveguide layout of a typical optical fiber used for communication. The fiber typically consists of a number of layers starting with the core as its central layer made out of doped glass. The middle layer typically consists of fused silica and is known as the cladding. The core and the cladding layers differ slightly in their refractive indices with the refractive index (RI) n_1 of core slightly higher than that of the cladding (n_2). This results in confinement of the majority of light inside the core due to total internal reflection (TIR). The outermost layer (shown in grey color in the figure) is usually a polymer layer known as a buffer layer and the primary function of this layer is to improve the mechanical strength of the optical fiber for better handling.

The optical fibers can be primarily categorized as single mode fiber (SMF) and multi-mode fibers (MMF) supporting only a single propagation mode or multiple modes, respectively. Both of these types are used to fabricate optical fiber sensors to be used in a wide range of applications due to the many inherent advantages that the optical fiber

sensors possess over the conventional electrical sensors [1][2][3]. The advantages are as follows:

- Immunity from electromagnetic interference
- Usability in corrosive environments
- Usability in harsh environments including high pressure and temperature
- Compact size and lightweight
- Multiplexing capabilities
- Low loss over long distance data transfer operations
- High sensitivity, large bandwidth and dynamic range
- Embeddability

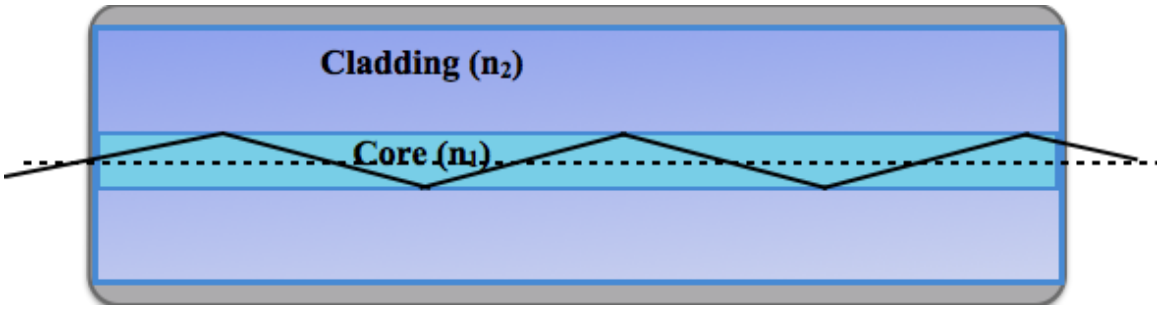

Figure 2.1 Schematic representation of the optical fiber as a waveguide under TIR conditions.

2.2 STRAIN SENSORS

Deformations produced by stresses on a material are measured by strain. Strain can be loosely categorized as shear strain and axial strain depending upon whether the strain is measured in angles with respect to the directions the strain is applied in or whether it is simply a measure of change in length in one specific direction. For the work presented in this dissertation, the focus has been on the axial strain measurement. Strain

sensors are used in a wide range of applications like fatigue testing, strain profiling, impact testing, load testing, cure monitoring etc. [4][5][6][7][8][9][10]. The most common fields that use these sensors include but are not limited to civil structure monitoring for bridges, dams, roads etc. and aerospace structures like airplane wings.

There are many types of strain sensors available, a brief review of these sensors is provided in the following sub-sections.

2.2.1 Electronic Sensors. Traditionally, electronic strain sensors are based on metallic resistance gauges. These gauges are mounted on the surface to be monitored by means of using glue, epoxy, ceramic cements or other similar adhesives. Change in the shape (elongation) of the metallic foil/wire results in the strain measurement. These type of sensors are useful at room temperature but with the increase in the temperature, resistance of the material changes as well making it difficult to measure precise strain due to mismatch in the elasticity of the host material and the gauge material. The applied strain is proportional to the resistance multiplied by a sensitivity constant of the material known as the gauge factor [11]. This gauge factor changes with temperature. Figure 2.2 shows a resistance based strain gauge surface-mounted on a composite material using epoxy.

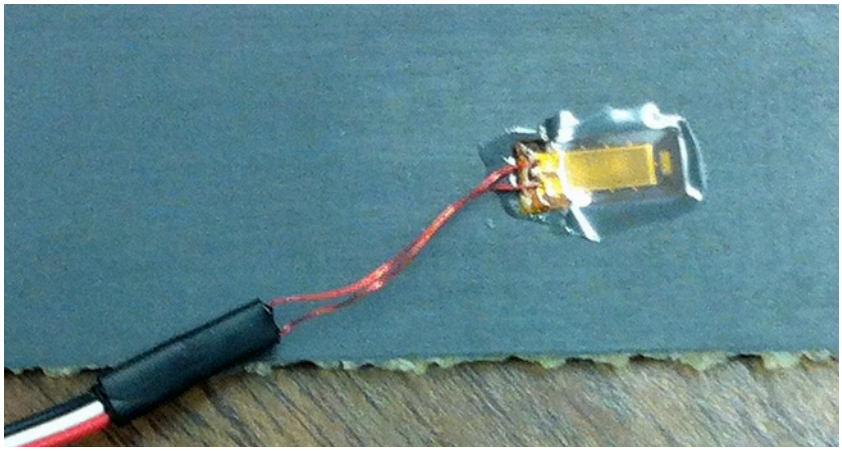

Figure 2.2 Resistance base strain gauge surface-mounted on a composite material.

Though some of the sensors developed using special material like silicon carbide (SiC) and silicon nitride (SiN) provide good resolution for temperature up to 700 ºC, the major concern with electronic sensors remain electromagnetic interference, temperature cross-sensitivity and inability to be embedded inside a material or structure for comprehensive structural monitoring.

2.2.2 Microelectromechanical Devices. Microelectromechanical systems (MEMS) are a popular technology for fabricating miniaturized sensors for strain, pressure, temperature measurement etc. MEMS devices consist of different modules like controllers, software, sensors and actuators communicating with each other to produce a desired measurement. MEMS sensors are formed in bulk by multiple growth layers of crystals on a substrate and subsequent etching [12][13].

The most common type of process used for strain measurement in MEMS is change in the resistance of piezoresistive material induced by the applied mechanical strain. The guage factor of the piezoresistive elements depends upon temperature, material, doping level, and crystallographic orientation [14][15].

In addition to offering flexible interrogation; optical as well as electrical, MEMS sensors offer bulk manufacturing due to batch manufacturing leading to low cost but temperature cross-sensitivity and packaging remains a concern. Like electronic sensors, the MEMS are also primarily intended for surface mounting applications and cannot be embedded inside a structure due to their intricate fabrication.

2.2.3 Pneumatic Sensors. Pneumatic strain sensors are based on the principle of pressure change dependence on the amount of a gas or a liquid passing through a pressure chamber. The change in the amount of a fluid is further dependent on the change induced by applied strain/pressure or other parameters to be measured. These sensors may be based on MEMS technology, electronic components or mechanical components. Though these sensors offer very high precision, they are usually much larger in size over other available sensors and it is very challenging to use them for structural health monitoring applications due to packaging issues and multi-component design [1][2][3][16].

2.2.4 Optical Fiber Sensors. Optical fiber sensors are in use for a number of applications like strain, temperature, refractive index measurement, etc. These sensors are fabricated by changing the physical structure of the optical fiber thus changing its

physical properties or waveguide properties or by manipulating the inherent differences in the properties of SMF and MMF optical fibers and combining these two to form sensors.

2.2.4.1 Fiber Bragg Gratings. Fiber Bragg gratings (FBG) are one of the most commonly used optical fiber sensors. Gratings consist of structures with periodic refractive index changes in general. An optical fiber grating consists of the periodic variations along the length of the SMF core resulting in periodic refractive index changes. In the case of a Bragg grating, the period of RI change is very short within the scale of the optical wavelength. This structure results in multiple reflectors resulting in successive coherent scattering. The strongest interaction occurs at the Bragg wavelength described by the Bragg condition. Equation 2.1 below defines the Bragg condition where λ_B is the Bragg wavelength, n_{eff} is the effective RI of the fiber and Λ is the grating period.

$$\lambda_B = 2n_{eff}\Lambda \tag{2.1}$$

The ambient parameters like temperature, strain, pressure, etc. change the effective RI or the grating period thus inducing changes in the reflection or transmission spectra. These changes can either be measured by monitoring power levels or wavelength shift.

The FBG can be fabricated using various methods. Point-by-point laser inscription where the laser beam is used to inscribe patterns on the core of the optical fiber at a specified period to change the local refractive index and ultraviolet masking technique where the RI changes at all locations are done at the same time, are the most commonly used methods [17][18][19].

FBG sensors offer additional advantages over the general advantages of an optical fiber including distributed sensing and flexibility for use in embedded applications. However, the Bragg gratings are intrinsically sensitive towards both strain as well as temperature. Thus, the cross-sensitivity is an issue while using these sensors at high temperatures.

2.2.4.2 Long-Period Fiber Gratings. Like the FBG, long period fiber gratings (LPFG) also have periodically modulated core refractive index. But in LPFG, the structure promotes coupling amongst the propagating core modes and co-propagating cladding modes unlike the FBG where the coupling is based on core interaction

primarily. This interaction results in formation of several attenuation bands in the transmission spectrum of the grating. These bands are located at discrete wavelengths resulting from coupling to different cladding modes. The center wavelength of the bands can be monitored to measure changes induced by induced strain, ambient temperature, stress, bend radius etc. Any of these changes will modify the phase-matching conditions for core-cladding modes coupling thus resulting in a change in the central wavelength of an attenuation band. Fabrication techniques used are similar to the FBG fabrication techniques. [20][21][22][23]

Inherent properties of the LPFG offer an extensive range of applications but a significantly long length (usually 30 mm or more depending upon the mode interaction required), sensitivity towards multiple local environment factors, and degrading mechanical optical strength make it difficult for use in harsh environment applications where high temperature, pressure, corrosive environment (changing refractive index) etc. are the key factors and cross-sensitivity poses a major concern.

2.2.4.3 Intrinsic Fabry-Perot Interferometer. A Fabry-Perot interferometer (FPI) comprises of a cavity where the cavity surfaces or walls can be any optical components. Optical fiber based FPI are loosely categorized as intrinsic FPI and extrinsic FPI. Creating two parallel internal reflectors inside the fiber forms intrinsic FPI. These reflectors may be formed by using laser inscription on the fiber core or by fusing a regular fiber with two other fibers with their end-faces metal coated. The middle fiber section forms the cavity and the metal coatings act as mirrors. Other structures include using arc-discharge to form one of the mirrors and the fused fiber end-face acts as the other mirror, HCl assisted etching to obtain internal mirrors, using a pair of FBG to form the cavity etc. [24][25][26][27]

IFPI sensors have been demonstrated for various applications like pressure, strain, temperature etc. They have an advantage over gratings since they are much smaller in size. Though IFPI sensors are good for embeddable applications, they are very sensitive to strain as well as temperature thus making cross-sensitivity an issue once again.

2.2.4.4 Extrinsic Fabry-Perot Interferometer. The extrinsic Fabry-Perot interferometer (EFPI) sensor's cavity consists of materials other than the fiber itself (giving it the name extrinsic) with fiber end faces forming the parallel cavity walls. The

EFPI-type sensors are better suited for strain monitoring applications with high ambient temperatures as opposed to Bragg gratings, LPFG and IFPI sensors because of the inherent low or negligible dependence on temperature. These rugged sensors have excellent noise-free performance and fatigue characteristics [6]. EFPI sensors are very small on the order of a few μm whereas grating-based sensors are on the order of mm.

The most widely used method for realizing the EFPI sensor is by epoxying two pieces of fiber, with cleaved ends, inside a hollow tube (glass or ceramic) and controlling the separation distance between the two fiber-ends. In some cases, the cleaved ends were polished and coated to increase the reflectance [27][28][29][30][31]. In addition to the cumbersome fabrication process and the calibration issues related to controlling the cavity gap, this design has limited thermal performance due to the thermal expansion of the tube and the temperature limitation of the epoxy, e.g. Loctite epoxy extra time pro (slow setting) is effective up to 150 °C once cured. Alternative approaches with low temperature sensitivities have been demonstrated by splicing a hollow-core fiber between two sections of single-mode fiber [32], by forming voids at splices between photonic crystal fiber and conventional single-mode fiber [33][34][35], and by laser-machining micro-cavities into single-mode fiber [36]. An EFPI sensor can also be fabricated using wet chemical etching in which diluted hydrofluoric acid forms a cavity in the tip of a multimode fiber and this cavity is fused with a single-mode fiber [37]. This latter EFPI alternative has good temperature characteristics, but it suffers from safety concerns during fabrication and from difficulty in controlling the etching rate, i.e. for calibrating the cavity length.

In this work, a micro-cavity EFPI strain sensor is fabricated using femtosecond (fs) laser micromachining to form the cavity and self-enclosed with a fusion splice. This sensor is less bulky than a tube-based EFPI, the fs-laser processing is fast and the resulting cavity length is precisely controlled. The performance is relatively temperature insensitive, thermally stable and the sensor is capable of operating in high-temperature applications.

2.3 SMART STRUCTURES AND OPTICAL FIBER SENSORS

Repair and maintenance of structures in developed countries demand a considerable amount of resources to be used each year. Recent years have seen a new development in the field namely embedded sensors as a smart structures technology. Embedding sensors while constructing new structures or repairing the old ones allows for continual monitoring of structural health thus giving an estimate of remaining utility. This capability provides an opportunity for preventive measures, e.g. performing repairs in time to prevent any major damage. Embedded sensors have been used for cure monitoring, fatigue detection, strain profiling, and temperature measurement [38][9].

Optical fiber based sensors have gained wide interest for structural health monitoring applications due to their compact size, immunity from electromagnetic interference, multiplexing capabilities etc. Different types of optical fiber sensors like Fiber Bragg gratings, extrinsic Fabry-Perot interferometric (EFPI) sensors, intrinsic Fabry-Perot interferometric (IFPI) sensors, long period fiber gratings, and combinations of these sensors have been used for monitoring strain, temperature, cure monitoring, and pressure in the field of structural health monitoring.

For composite laminates, embedding optical fiber sensors is very easy to implement with no material degradation. With rise in the use of composites in the aerospace and civil structures, embeddable sensors are sought after more than ever. Optical fiber sensors have gained wide interest for in-situ monitoring of the composite laminates and the most common parameter to be monitored for evaluating the in-service condition of the composite laminates is strain [38][40][41]. Composites in aerospace applications can be exposed to harsh service conditions, e.g. high strain and fluctuating temperature. Thus, structural monitoring can provide valuable information regarding the in-service behavior of these materials.

In the work presented in this dissertation, high performance Bismaleimide (BMI) composite laminates are used. These composites are used in aerospace applications due to their superior strength and mechanical performance at elevated temperatures [41][42][43]. This composite was developed recently and has not yet been investigated significantly. We are aiming at providing more insight into the strain characteristics of BMI by using optical fiber sensors.

2.4 MOTIVATIONS AND OBJECTIVES

Smart materials like carbon fiber composites are used in aerospace and civil infrastructure monitoring applications where the sensors are required to monitor strain profiles in elevated temperature environments. These requirements present an appropriate opportunity for fs-laser micromachining to fabricate optical fiber sensors. Fs-laser fabrication yields thermally stable structures that can withstand higher temperatures as compared to the regular optical fiber sensors.

The objective of this research was to fabricate optical fiber sensors using fs-laser micromachining for embeddable applications that would resolve some of the current fabrication issues like size, ease-of-fabrication, precise sensor length etc. These sensors should also be easy-to-handle and easy-to-embed for structural health monitoring applications. Following are the specific objectives that needed to be met with this research:

- Development and demonstration of a novel extrinsic Fabry-Perot interferometric (EFPI) sensor using fs-laser micromachining. The strain sensitivity and high temperature survivability of the sensor are to be demonstrated experimentally.
- Demonstration of embeddability of the fabricated sensors for structural monitoring applications, specifically for fiber reinforced composites.
- Strain monitoring of the Bismaleimide (BMI) composite samples using the fabricated sensors.
- Development and demonstration of an optical fiber sensor fabricated using fs-laser micromachining for simultaneous measurement of strain and temperature.
- Specific long-term application: observation of strain and temperature effects on a composite based airplane wing.

2.5 INNOVATIONS AND CONTRIBUTIONS

Major scientific and technical contributions of this work include the following:

- A new type of embeddable Extrinsic Fabry-Perot Interferometer sensor using fs-laser micromachining was fabricated. This sensor was fabricated for applications requiring embeddable strain sensors with minimal temperature interference. The micro-cavity based EFPI sensor demonstrated temperature insensitive strain sensing.
- A hybrid sensor using the EFPI, and IFPI was fabricated for the simultaneous measurement of temperature and strain. The temperature and strain components were extracted using a simple sensitivity matrix. This sensor was fabricated for strain sensing applications at elevated temperatures requiring embeddable sensors. With many unique advantages such as linear response towards strain and temperature, small size, immunity towards electromagnetic interference, flexibility of fabrication, ease of handling, high temperature survivability, usability in corrosive environment, and low loss over long distance data transfer operations, these sensors can be used for many embedded as well as non-embedded applications.
- Embeddability of both the EFPI and hybrid sensors was demonstrated using carbon fiber/Bismaleimide (BMI) polymer by embedding the sensors in between the middle layers of the BMI laminates before the curing process. Both types of the sensors survived the curing process. BMI is a relatively new material and any research aimed at providing more data about the material response is highly desirable.
- For the first time, the strain characteristics of the carbon fiber/Bismaleimide (BMI) polymer were observed using the optical fiber sensors. The BMI composites are highly sought after for their flexibility and high strength. These composites are under investigation for their feasibility in aerospace applications, specifically for their usage in manufacturing airplane wings to study the dynamics of air pressure and temperature changes exerted on the wings during take - off and landing procedures.

- The curing properties of the BMI polymer were also studied using the optical fiber EFPI sensors. The in-situ monitoring was performed during the sample manufacturing process. The characteristics obtained by analyzing the data obtained using the EFPI sensors produced results very similar to the expected theoretical curing cycle of BMI.

The presented fs-laser machined cavity based sensor is similar in structure to the chemically etched [37] and the open cavity design [36]. The advantages of the described cavity sensor include compact size, precise cavity length control, easy-to-handle structure, embeddability, and negligible temperature cross-sensitivity making this sensor an ideal selection for embeddable applications in the field of composite structures.

3. FABRICATION AND THE OPERATIONAL PRINCIPLES OF THE SENSORS

This section includes an introduction to the extrinsic and intrinsic Fabry-Perot interferometer based sensors and a brief review of the fabrication techniques most commonly used. Detailed fabrication of the sensors using the fs-laser micro machining is explained along with the sensing mechanisms, and the typical reflection spectra characteristics are discussed. Performance of the two sensors at high temperatures is discussed along with their temperature sensitivities. Also included in this section is the procedure that was followed to manufacture the BMI samples used for embedded sensors' testing. Applications of the EFPI and IFPI sensors are also discussed.

3.1 INTRODUCTION TO THE EXTRINSIC AND INTRINSIC FPI

The Fabry-Perot interferometer sensors are usually categorized into extrinsic or intrinsic. Though both types of the structures consist of a cavity separating two reflecting surfaces, formation of the cavity is different. The reflecting surfaces can be any optical components. The most common and simple way of achieving the FPI structure is by using the cleaved ends of an optical fiber as reflectors. To produce a high quality of interference signal (also known as high fringe visibility), single mode optical fibers are used due to their small numerical aperture (NA). The small NA helps retain a small divergence angle in the light beam exiting out of a fiber core. In case of the EFPI, the cavity exists outside of the fiber and thus the medium of the cavity is air. The EFPI sensor is fabricated by aligning two cleaved pieces of the optical fiber together and controlling the gap between the reflecting surfaces of the two fibers creates the cavity. Different methods to achieve this are described in the following sections. On the other hand, the reflecting surfaces forming the cavity are on the fiber core or inside the fiber itself in the case of the IFPI. The cavity medium is same as that of the fiber. Similar to the EFPI, there are different methods to fabricate IFPI sensors. These methods are also discussed in the following sections.

3.2 FABRICATION TECHNIQUES – REVIEW

A brief review of different fabrication techniques commonly used to fabricate EFPI and IFPI sensors are discussed in the following sections. Limitations of the existing techniques and advantages of using femtosecond laser micro machining are also discussed.

3.2.1 Extrinsic Fabry-Perot Interferometer Sensors. The most widely used method for realizing the EFPI sensor is by epoxying two pieces of fiber, with cleaved ends, inside a hollow tube (glass or ceramic) and controlling the separation distance between the two fiber ends [28][29][30][31]. In addition to the cumbersome fabrication process and the calibration issues related to controlling the cavity gap, this design has limited thermal performance due to the thermal expansion of the tube and the temperature limitation of the epoxy, e.g. Loctite epoxy extra time pro (slow setting) is effective up to 150 °C once cured. An EFPI sensor can also be fabricated using wet chemical etching in which diluted hydrofluoric acid forms a cavity in the tip of a multimode fiber and this cavity is fused with a single-mode fiber [37]. This EFPI alternative has good temperature characteristics, but it suffers from safety concerns during fabrication and from difficulty in controlling the etching rate, i.e. for calibrating the cavity length.

Figure 3.1 (a) shows a traditional EFPI design in which the cavity is formed between the end faces of optical fiber that are aligned with an epoxied capillary tube [28][29][30]. Figure 3.1 (b) shows the micro-cavity EFPI in which the cavity is formed in the fiber itself and a second fiber is fusion spliced to self-enclose the cavity. The smaller gage length allows the latter sensor to more closely approximate a point sensor. Also, the tube component causes the former design to be bulkier and to have a more complex fabrication than the micro-cavity design. Note that the exact gage length and the initial gap length are more difficult to determine for the traditional design. Hence, calibration is an issue.

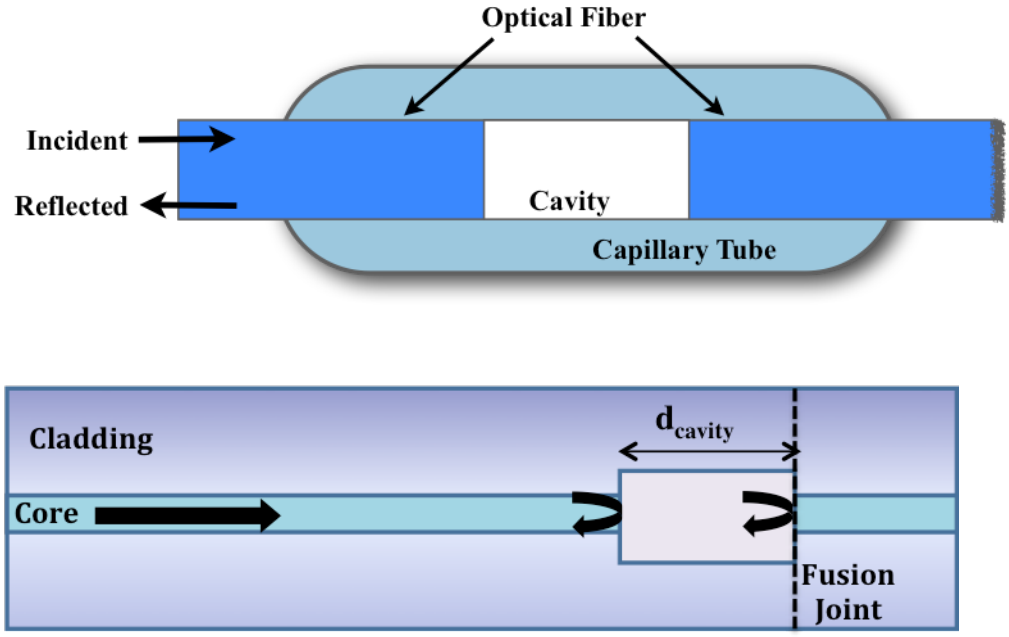

Figure 3.1 EFPI structure. (a) Traditional tube-based EFPI sensor and, (b) Micro-cavity EFPI sensor.

3.2.2 Intrinsic Fabry-Perot Interferometer Sensors. A typical IFPI consists of two reflecting surfaces inside the optical fiber. Different structures of the IFPI have been demonstrated over the years; consisting only of a single mode fiber (SMF), consisting of both a SMF and a multi-mode optical fiber (MMF), combination of fiber Bragg gratings (FBG) and SMF, etc. [25][26][44][45]. Figure 3.2 shows the diagram of an IFPI with reflecting surfaces on the core of a SMF separated by a distance 'd' that acts as the cavity length.

Different methods of fabricating the IFPI sensors have been explored over the years. One of the methods uses arc-discharge to create a thin reflecting surface on the single mode fiber end by exposing the cleaved fiber end to arc discharge multiple times. This fiber is then fusion spliced to another piece of fiber with a cleaved end that acts as the second reflecting surface thus forming the cavity [26].

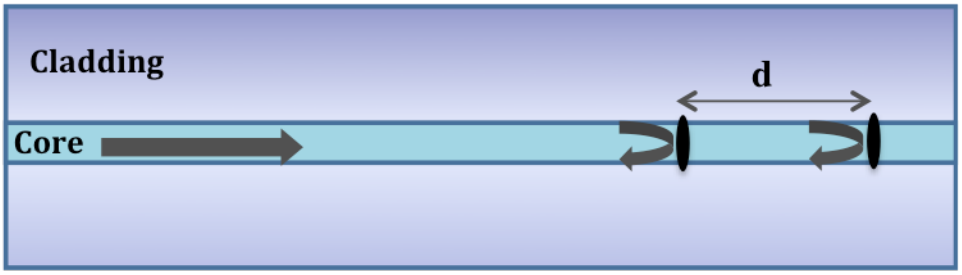

Figure 3.2 Schematic of an IFPI sensor consisting of two reflecting surfaces on the fiber core.

In another method, the IFP cavity consists of a FBG reflector and mirrored end-face of the fiber on which the grating was inscribed [44]. The most common and simple method involves fusion splicing a lead-in SMF to a section of MMF, the MMF fiber section is cleaved at a desired length, 'd' and fusion spliced to another piece of SMF. The two fusion points (interfaces of the SMF-MMF) act as the reflecting mirrors [45]. Hydrofluoric acid etching has also been used to realize the IFPI sensor [25].

Though extensively used, these methods have their limitations. The arc-discharge method for example, is time consuming and a precise control of the heated thin film's shape might be difficult to control. Chemical etching suffers from safety concerns during fabrication and controlling the etching rate is another challenge. Femtosecond laser micro machining provides an easy and repeatable process to overcome these challenges.

3.3 FEMTOSECOND LASER MICRO-MACHINING

Femtosecond laser micro machining was used to fabricate the EFPI and the IFPI sensors used for the results presented in this dissertation. This fabrication process offers a faster, easier, and repeatable solution over the conventional methods.

Figure 3.3 shows the actual laboratory integrated fs-laser micromachining system and Figure 3.4 shows the schematic representation of the system for better understanding. The fs-laser system consists of a regenerative amplified Ti:Sapphire laser (maximum

output of 1 W) that operates at a center wavelength of 800 nm with the repetition rate and a pulse width of 250 kHz and 200 fs, respectively. A combination of wave-plate, polarizers and neutral density filters were used to reduce the power to 0.4 μJ per pulse for the fabrication. An objective lens with 20X magnification and 0.4 numerical aperture was used to focus the laser beam on the tip of the fiber. A step size of 1 μm per scan was chosen for precise control of cavity dimensions.

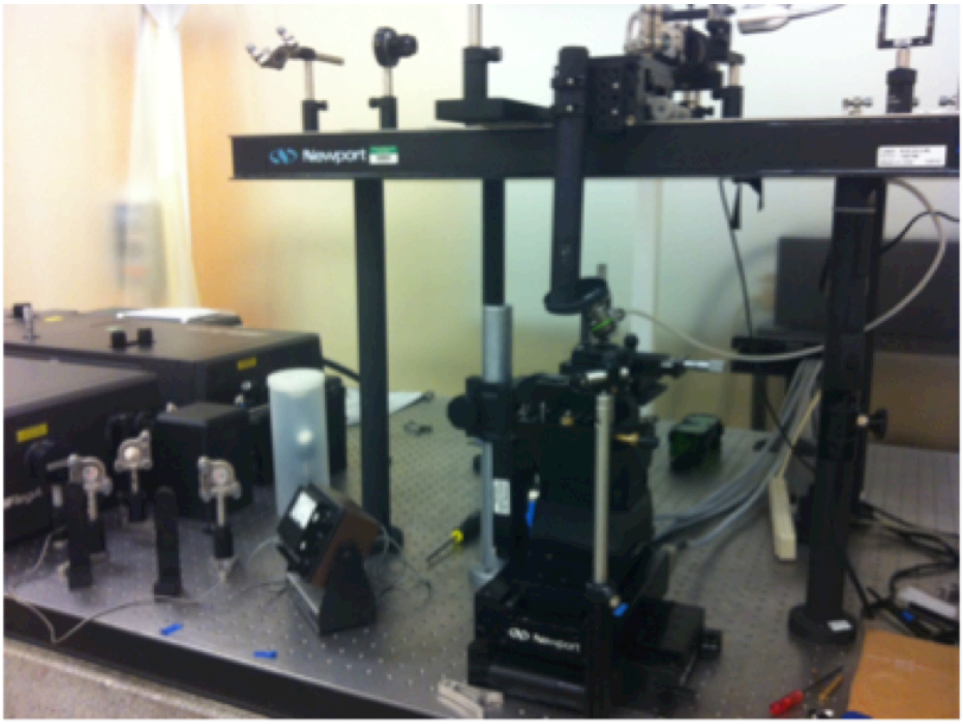

Figure 3.3 Laboratory integrated femtosecond laser micro-machining system.

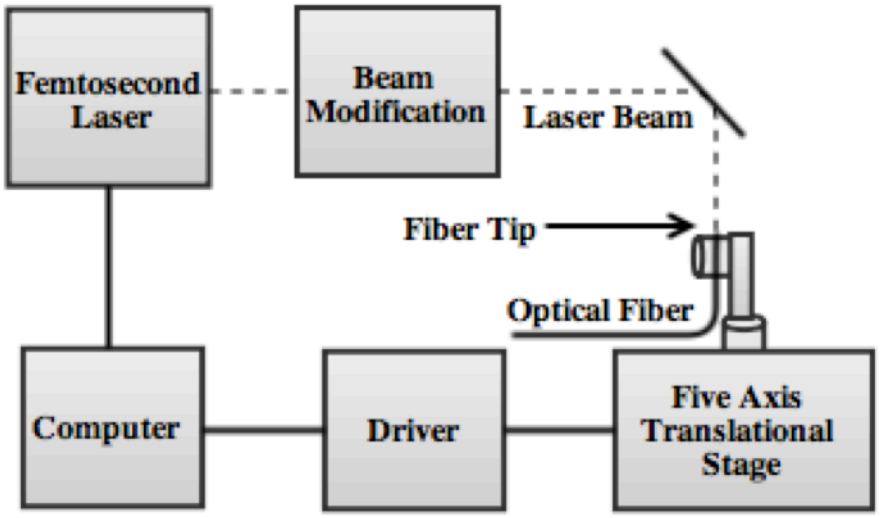

Figure 3.4 Schematic diagram of the femtosecond laser micro-machining system.

3.3.1 Extrinsic Fabry-Perot Interferometer Sensor Fabrication. To fabricate an EFPI sensor, the single-mode fiber was cleaved and the fiber was mounted on a computer-controlled five-axis translation stage (Aerotech, Inc.) with a resolution of 1 µm as shown in Figure 3.4. The fs laser was focused on the fiber tip and a cavity of depth 36 µm was precisely ablated as shown in Figure 3.5 (a). A constant flow of pressurized air was targeted at the fiber tip to remove the debris being generated during the fabrication process for a better quality of fabrication. The sensor fabrication was completed by fusion splicing (Sumitomo Type-360 fusion splicer) another single-mode fiber to the fiber with the cavity on the tip; see Figure 3.5 (b). To avoid increasing the curvature of the cavity walls and decreasing the cavity depth during the fusion splice process, multiple combinations of arc duration, arc power and overlap were tested. The best-suited combination results in a cavity of dimensions 65 µm x 65 µm x 35 µm. The cavity depth reduces slightly because of the fusion splicing process as the fibers are heated and fused together. Though the cavity walls have a slight curvature towards the second reflective wall, the width of the cavity is enough to avoid any curvature close to the core of the fiber. Figure 3.6 shows the SEM images of the ablated cavity.

The resulting structure is easier to handle and the cavity length can be controlled precisely due to the high resolution of the translational stage. The tube component causes the former traditional designs to be bulkier and to have a more complex fabrication than the micro-cavity design. Note that the exact gage length and the initial gap length are more difficult to determine for the traditional design. Hence, calibration is an issue.

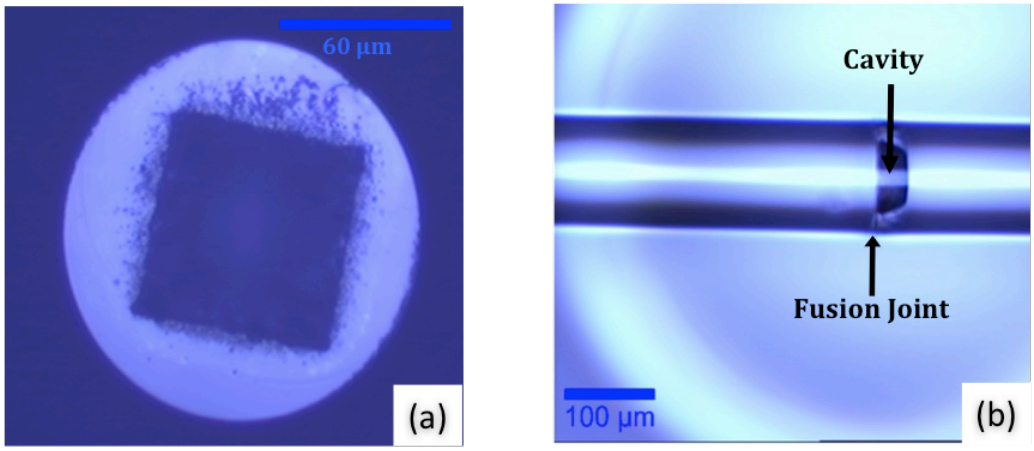

Figure 3.5 Confocal microscopic images of the EFPI. (a) Image of the micro-cavity machined on the tip of the fiber. (b) Image of the EFPI sensor.

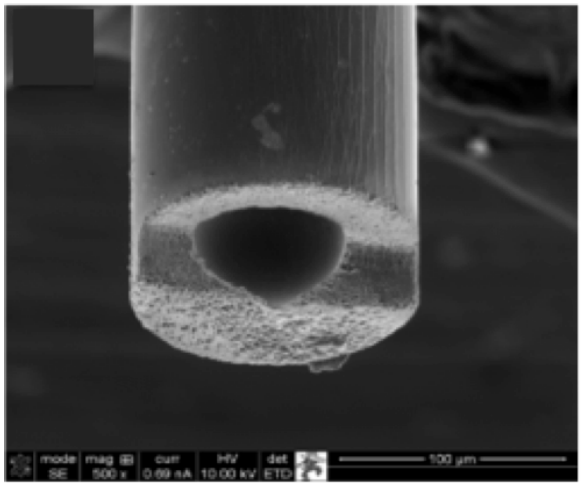

Figure 3.6 SEM image of the cavity ablated using the fs-laser micro-machining system.

3.3.2 Intrinsic Fabry-Perot Interferometer Sensor Fabrication. Using the femtosecond laser micro machining for the fabrication of the IFPI sensors makes the process easier, faster and repeatable along with making the structure robust due to the fact that it is a single material structure without any joints. The same set up as described in the Figure 3.3 was used for fabricating the IFPI sensors with a change in the fiber orientation and placement. A small portion of the single mode optical fiber was stripped off its buffer layer and placed inside a container filled with water fixed on the translational stage. A fiber holder held the fiber in place. The water immersion was used to aid the laser beam in focusing onto the core of the fiber. Liquid immersion minimizes the refraction in order to achieve localized spots.

Two types of structures were used to fabricate the IFPI sensors. Figure 3.5 shows the microscopic images of both the structures. Figure 3.7 (a) shows a 2-cuboid structure where two-cuboids are formed to create the reflecting surfaces inside the fiber aligned with the core at the center of the structures. The separation distance between the two reflecting surfaces forms the cavity. Figure 3.7 (b) shows the second type of structure where a 2-point structure forms a cavity. Sufficiently large light intensity focused by the laser beam causes nonlinear absorption of the laser energy. Multi-photon absorption leads to avalanche ionization forming highly excited and spatially localized plasma as the energy is released via micro-explosions. Polarization dependent effects result in elliptical shape of refractive index modulations [46].

3.4 THEORY AND OPERATIONAL PRINCIPLE

The theory and operational principle of the EFPI and IFPI sensors are discussed in the following sub-sections.

3.4.1 EFPI – Sensing Mechanism And Characteristics. The overall optical response for a Fabry-Perot cavity depends on multiple-beam interference in light transmitted and reflected from the two ends of the cavity. This periodic response is modulated by the wavelength and optical path (gap) length [47]. The EFPI response is dependent on any parameter changing the cavity optical path length. For the bare sensor with no applied strain, e.g. a sensor not attached to a structure to be measured, changes in

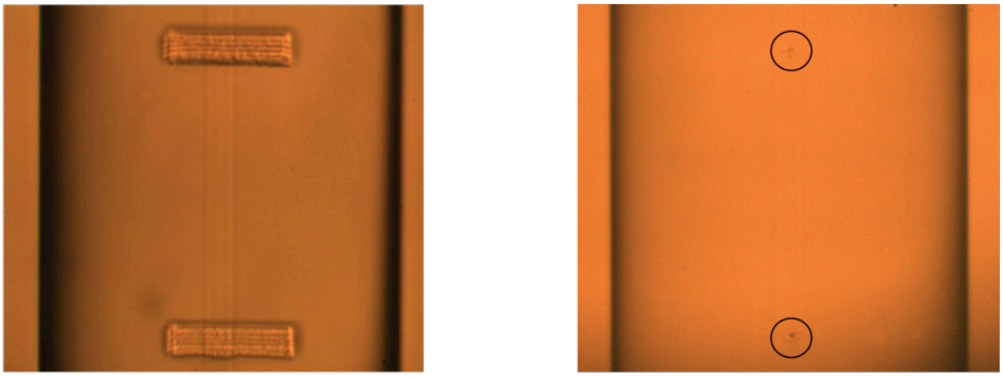

Figure 3.7 Microscopic images of the IFPI sensor. (a) Microscopic image of a 2-cuboid structure IFPI. (b) Microscopic image of a 2-point structure IFPI.

ambient temperature 'T' induces a change 'Δd' due to the thermal expansion of the silica fiber. For a traditional EFPI, a strain sensor with an air gap of length d, the gage length is approximately the tube length L and the measured strain is ΔL/L = Δd/d. Figure 3.8 shows the micro-cavity EFPI in which the cavity is formed in the fiber itself and a second fiber is fusion spliced to self-enclose the cavity. As a strain sensor with an air gap of length d, the gage length is the cavity gap length d and the measured strain is Δd/d. The smaller gage length allows this sensor to closely approximate a point sensor.

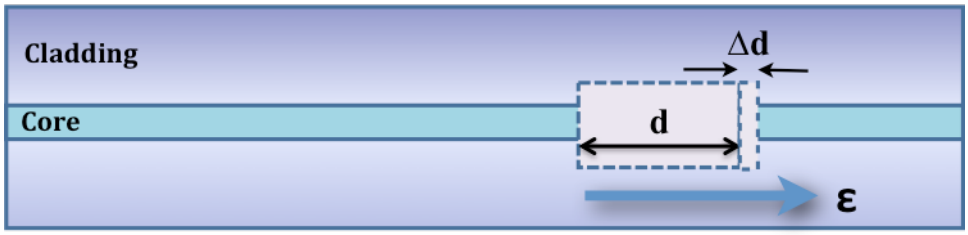

Figure 3.8 Elongation in the cavity of the EFPI sensor by the application of strain along the fiber axis is shown.

The micro-cavity EFPI has two glass-air interfaces with low reflectivity that produce a sensor with low finesse *F*. Thus, it can be modeled as a two-beam interferometer. The following method is known as the Phase tracking method and has been used to measure and evaluate the sensor response. The interference signal I_r, resulting from two reflections with intensities I_1 and I_2 can be given as the following equation where d is the cavity length, n is the refractive index of the fiber core, ϕ_0 is the initial phase of the interference, and λ is the optical wavelength in vacuum:

$$I_r = I_1 + I_2 + 2\sqrt{I_1 I_2}cos\left[\frac{4\pi}{\lambda}(nd) + \phi_0\right] \quad (3.1)$$

Since the cavity material is mostly air, the refractive index n is 1 and thus, the reflectance (ratio of the output signal irradiance I_R to the input signal irradiance I_i) is [47]

$$I_r/I_i = F\frac{\sin^2\left(2\pi d/\lambda\right)}{\left[1+Fsin^2\left(2\pi d/\lambda\right)\right]} \quad (3.2)$$

The condition for destructive interference is as given below where m is an integer.

$$4\pi d/\lambda = (2m+1)\pi \quad (3.3)$$

For two adjacent wavelength minima, the following condition is obtained:

$$4\pi d/\lambda_2 - 4\pi d/\lambda_1 = (2m+1)\pi - [2(m+1)+1]\pi = 2\pi \quad (3.4)$$

Note that the cavity length, d can be calculated from adjacent minima at λ_1 and λ_2 as,

$$d = \lambda_1\lambda_2/2(\lambda_2 - \lambda_1) \quad (3.5)$$

Demodulation of the micro-cavity EFPI response can be done the same as for traditional EFPI types.

Any change in the cavity length – positive or negative brings a proportional wavelength shift in the reflection spectrum. Thus the strain, ε can be calculated as follows:

$$\varepsilon = \Delta d/d = \Delta\lambda/\lambda \quad (3.6)$$

A typical reflection spectrum of an EFPI is shown in Figure 3.9. A shift of Δλ in the reflection spectrum that resulted after the EFPI sensor was subjected to a 500 με of strain is also shown.

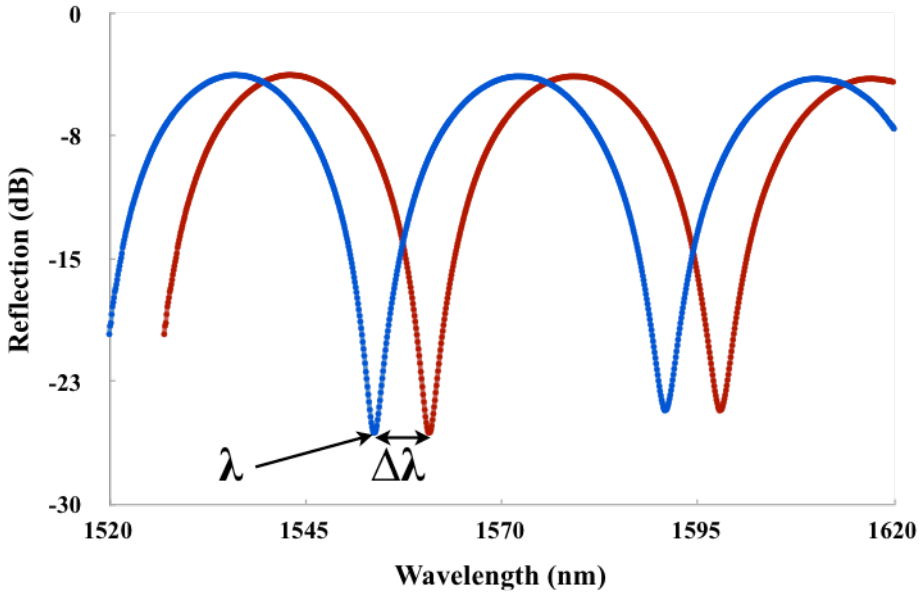

Figure 3.9 Typical spectrum of an EFPI sensor and the wavelength shift due to the application of strain are shown.

3.4.2 IFPI – Sensing Mechanism And Characteristics. Sensing operation of the IFPI sensor works the same way as the EFPI sensor for the strain sensing. The strain can be calculated using Equation 3.6. But unlike the EFPI, the temperature sensitivity of the IFPI sensor is high and is given by Equation 3.9. Figure 3.10 shows the typical reflection spectrum of the IFPI sensor. The spectrum shown below corresponds to a cavity length of 350 µm. The reflectors for the IFPI cavity are created inside the fiber and thus it is easier to form a longer cavity. Longer cavity length means a larger number of fringes and thus the ability of sensing smaller changes in the wavelength.

3.5 TEMPERATURE SENSITIVITY

High temperature survivability of the silica sensors and temperature sensitivity comparison of the EFPI and IFPI sensors will be discussed in this section.

3.5.1 High Temperature Survivability. The EFPI and IFPI sensors were tested for their temperature sensitivities by exposing them to temperatures as high as 800 ºC. Due to the low coefficient of thermal expansion (CTE) of the silica, the sensors fabricated using the single mode optical fibers can survive high temperatures of up to 1000 ºC. Temperature sensitivities of the EFPI and IFPI sensors were found to be 0.59 pm/ºC and 14.9 pm/ºC, respectively. Detailed results for the temperature testing will be presented in Section 4.

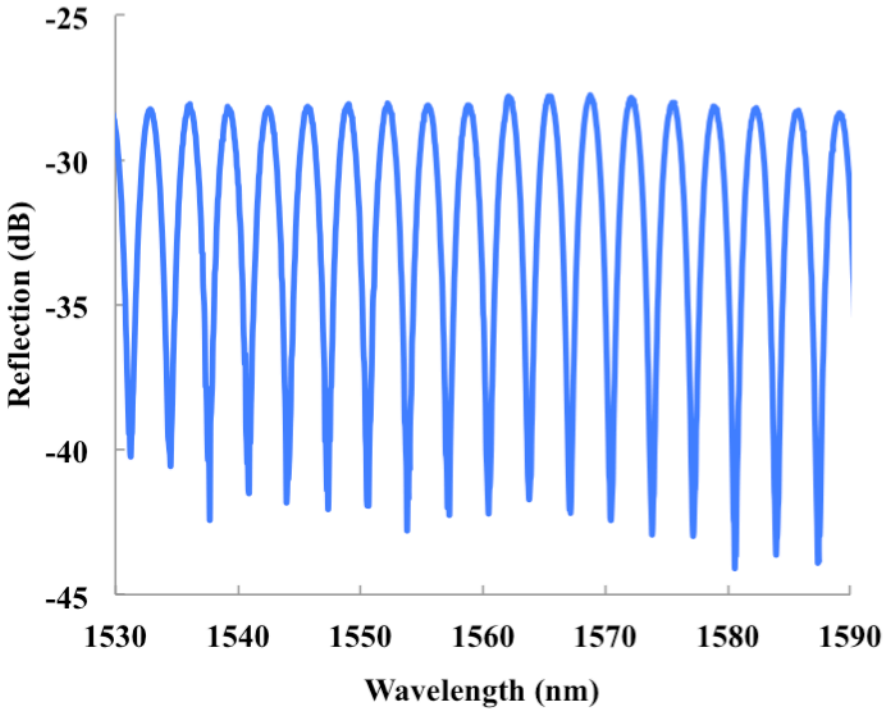

Figure 3.10 Typical reflection spectrum of an IFPI sensor.

3.5.2 Temperature Sensitivity of EFPI. Cavity length change due to temperature increase depends on the thermo-optic coefficient, α_{TO}, of the material inside the cavity and the CTE, α_{CTE} of silica. Temperature dependence of the wavelength for a Fabry-Perot cavity is given by the following equation [48][49]:

$$\boldsymbol{K = (\alpha_{TO} + \alpha_{CTE})\lambda} \quad (3.7)$$

Since the cavity in micro-cavity EFPI sensor does not have any material inside it except air and the coefficient of thermal expansion for silica (0.55 x 10^{-6}/ºC) is small [50], the temperature dependence is minimal and can be expressed as following:

$$\boldsymbol{K_{T,EFPI} = (\alpha_{CTE})\lambda} \quad (3.8)$$

Hence, the single-mode silica fiber EFPI is an ideal candidate for high-temperature applications. The smaller gage length and the absence of epoxy reduce the influence of temperature on the micro-cavity EFPI performance further.

3.5.3 Temperature Sensitivity of IFPI. As discussed in the section above, the temperature dependence of a Fabry-Perot cavity expansion is given by Equation 3.7. In the case of an IFPI cavity, the structure is inscribed inside the fiber and thus the cavity consists of the fiber material itself, silica in this case and thus the temperature sensitivity can be expressed as following:

$$\boldsymbol{K_{T,IFPI} = (\alpha_{TO} + \alpha_{CTE})\lambda} \quad (3.9)$$

The thermo-optic coefficient of silica is 8.3 x 10^{-6} /ºC. This added component results in higher temperature sensitivity of the IFPI sensor. Theoretically, IFPI is 16 times more sensitive to temperature compared to the EFPI sensor if the fiber material is silica. Experimental results to show the sensitivity comparisons are discussed in Section 4. These results demonstrated that the IFPI sensor was about 25 times more sensitive to the temperature as compared to the EFPI sensor.

3.6 MANUFACTURING BMI SAMPLES FOR EMBEDDED SENSORS

For embedding the sensor, six-layer unidirectional laminates were fabricated (12 in. x 1 in.), using IM7/AR4550 prepreg (composite sheets), by out-of-autoclave process. The prepreg sheets are useful for bulk manufacturing of composite material. These sheets consist of composite fibers with epoxy already laid on them. A sensor was embedded

between the central layers. The prepreg layup was cured at 190.55 ºC for two hours. The embedded sensor was used to perform cure monitoring. The glass transition temperature (271 ºC) of the BMI resin used to bind the sample limited the upper limit of the temperature tested. Table 3.1 lists the sample size of the laminates used and some properties of the BMI resin and composite.

Figure 3.11 below shows the assembly used to manufacture the BMI samples and to monitor the cure process. First, three layers of BMI prepreg were placed on an aluminum mold. The optical fiber sensor was then placed in the center to avoid any edge effects. Three more layers of prepreg were placed followed by a layer of Ethylene tetra-flouro-ethylene (ETFE) release film. A resin dam was placed around the parameter of the laminate along with the edge bleeder. The resin dam prohibits the melted resin that leaks out of the prepreg sheet to flow onto the mold and makes the removal of the sample easier. The layup was then covered by a breather fabric and sealed using a vacuum bag under full atmospheric pressure. The layup was placed in an oven for curing the sample. Detailed pictorial representation of each step leading up to the manufacturing process can be seen in Appendix A.

Table 3.1 Properties of the BMI resin/composite.

Sample size used for embedding the sensor	12 in. x 1 in.
Glass Transition Temperature	271 ºC
Cure Temperature	190.55 ºC
Tensile Modulus	20.6 Mpsi
Major Poisson Ratio (ν_{12})	0.29

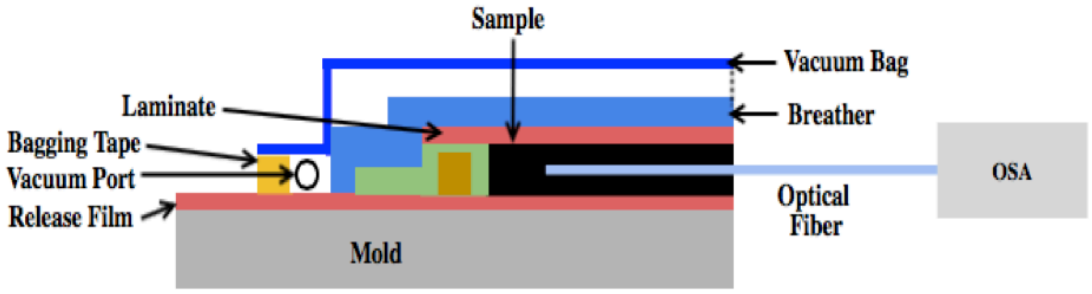

Figure 3.11 The assembly used to manufacture the BMI samples and to monitor the cure process.

Figure 3.12 shows the arrangement of the BMI laminate layers and the sensor placement. For results presented here, six-layer unidirectional laminates were fabricated (12 in. x 1 in.) using IM7G/AR4550 prepreg by out-of-autoclave process. A sensor was placed between the central layers in the middle to avoid any edge effects. The approximate location of the sensor was at [6 in., 0.5 in.]. A heat shrinking tube (protective tube) was used at the egress point to protect the sensor from breaking. The prepreg layup was cured at 190.56 ºC for two hours. Once cured, the embedded sensor was used to observe. The composite fibers in the laminate sheets were aligned along the length of the optical fiber. SEM images of the embedded sensor are shown in Figure 3.13. The sample was cut across its width and polished slightly to obtain the SEM images. The images shown here are of post-tested samples. The apparent inner circle marks the end-face of the optical fiber sensor whereas the outer circular lining is coagulated resin around the fiber. The irregular structure of the fiber material results from the roughly broken fiber during the sample cutting process. The position of the embedded sensor is marked in the Figure 3.13 (a). The BMI material can also be seen in this figure, the carbon fibers are too small to be seen discretely however.

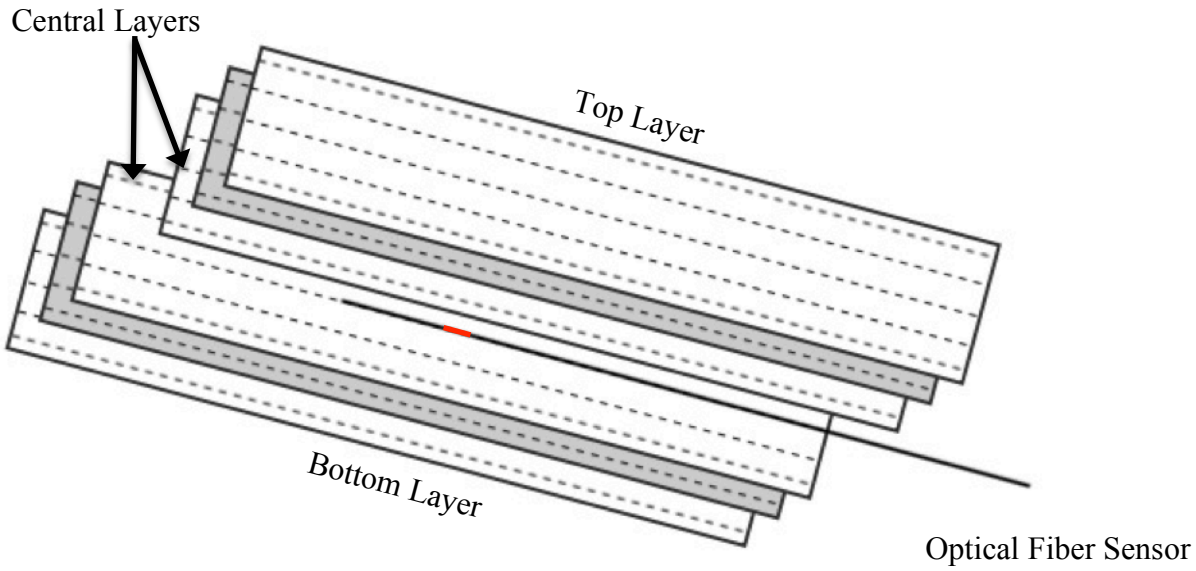

Figure 3.12 Embedded sample layout with the sensor embedded in the middle.

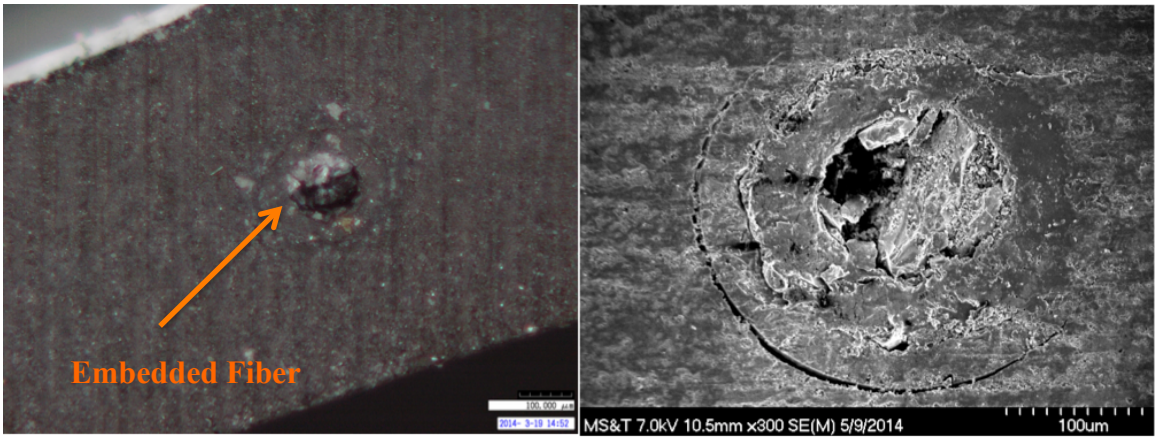

Figure 3.13 SEM images of the embedded sensor. (a) Embedded sensor inside BMI material. (b) Enlarged SEM image of the embedded sensor.

3.7 CONCLUSIONS

In this section, the fabrication of the EFPI and IFPI sensors was discussed. The fs-laser micro machining was used to fabricate the two sensors allowing for an easier, faster

and repeatable process. Changes like induced strain and increase in temperature reflecting a corresponding shift in the refection spectra of the two sensors were also discussed. The relevant equations for the calculation of the cavity length and the applied strain were also presented and explained. The fs-laser fabricated sensors generate reflection spectra with good fringe visibility. Higher temperature sensitivity of the IFPI sensor, over the EFPI sensor, due to its dependence on both CTE and thermo-optic coefficient of silica was also discussed.

4. EXPERIMENTAL SET UP AND RESULTS

This chapter includes the details of the experiments conducted to obtain results for EFPI and IFPI sensors in non-embedded and embedded applications. The experimental set up and the results obtained are discussed for strain and temperature measurements. Results obtained for the implementation of the EFPI sensor for cure monitoring are also discussed. The EFPI sensors that produced these results were very similar in terms of cavity length, fringe visibility, and background noise. Fringe visibility of the sensors for which the results are presented here ranged from 12 to 20 dB with a background loss of 6 to 9 dB.

4.1 EXPERIMENTAL SET UP FOR STRAIN SENSING

The experimental set up is described for strain, and temperature monitoring using non-embedded, and embedded sensors.

4.1.1 Non-Embedded Sensors. The same experimental set up was used for both non-embedded EFPI and IFPI sensors to apply strain and obtain in-situ results. Figure 4.1 shows the instrumentation used for sensor testing. A 100-nm broadband source was used to provide the input into the fiber via a 3-dB coupler. The signal reflected back by the EFPI cavity is collected back using the 3-dB coupler and an optical spectrum analyzer (OSA) then records the wavelength spectra. The sensor was fixed onto a translational stage (Newport) at one end and onto a fixed block on the other end. The axial strain was applied in steps of 100 με by applying elongation along the fiber axis. A certain amount of pre-strain was applied in order to make sure that the sensor was stretched and not loose before starting the experiment. Pre-strain was calibrated to be read as 0 με.

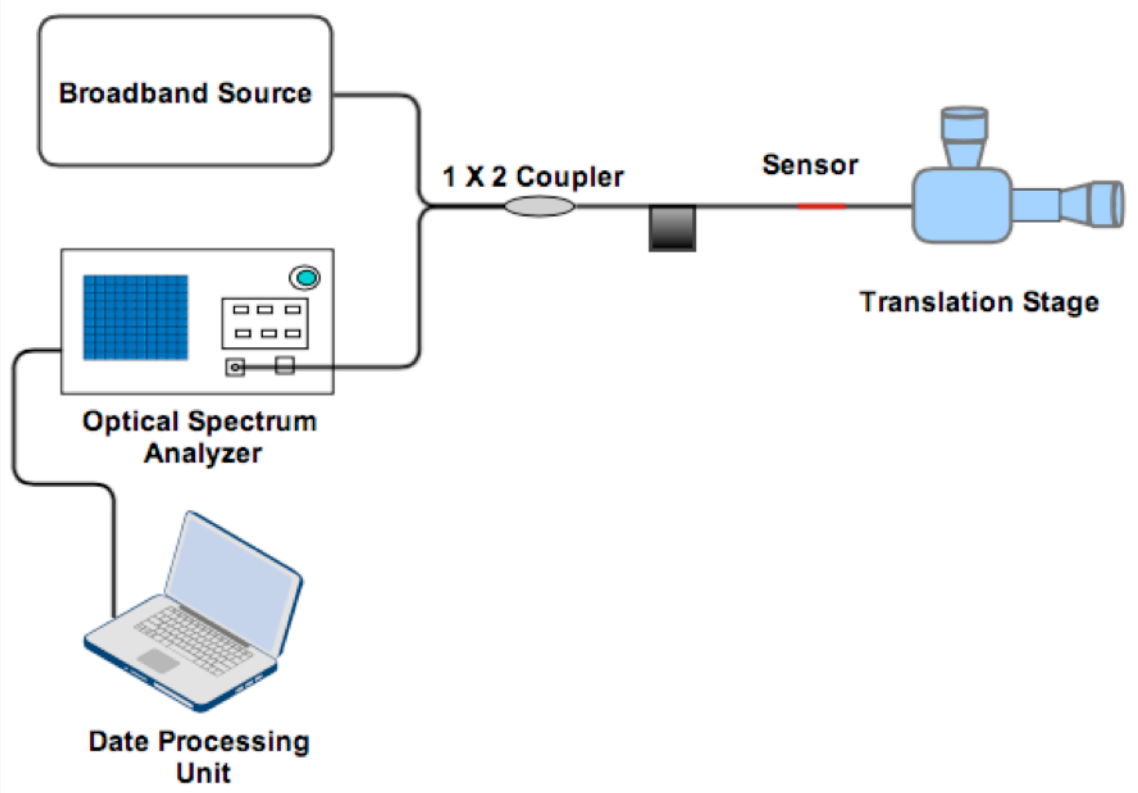

Figure 4.1 Experimental set up for strain testing of non-embedded sensors

4.1.2 Embedded Sensors. For the embedded sensor, an INSTRON 5985 tensile test machine was used to apply tensile load on the embedded sample. An axial strain was induced along the optical fiber/sensor axis resulting in a wavelength shift in the reflection spectra. These spectra were then recorded using an optical spectrum analyzer. The recorded data was then processed to find the corresponding wavelength shift for each applied strain step. Figure 4.2 shows the placement of the BMI composite sample with embedded sensor between the grips of the test equipment. The optical fiber can be seen coming out at the right side of the sample; the shrinking tube used to prevent the fiber from breaking at the egress point can also be seen. The figure shows a longitudinal split as a result of the substrate failure at which point the sensor also broke. The split might have resulted due to a non-perfect alignment of the laminate sheets.

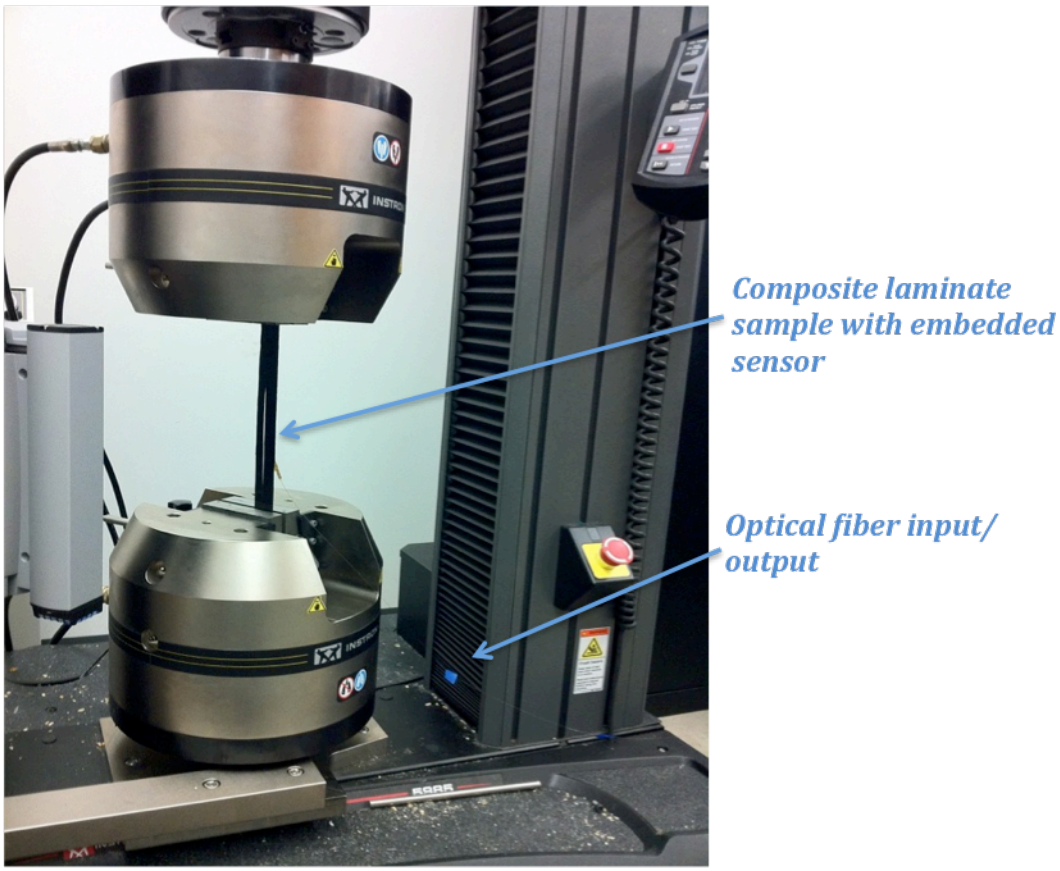

Figure 4.2 Experimental set up for strain testing of embedded sensors

4.2 EXPERIMENTAL RESULTS FOR STRAIN SENSING

In this section, experimental results for strain testing for EFPI and IFPI sensors are presented and discussed.

4.2.1 EFPI Sensor. Strain sensitivity responses of the non-embedded and the embedded sensors at room temperature are presented in Figure 4.3. As can be observed from the plot, the embedded sensor has a lower slope (0.6 pm/με) as compared to the non-embedded sensor (1.5 pm/με). A cycle of tensile test was performed for the embedded sensor where the applied strain was increased up to 4000 με and then

decreased to a zero strain state in steps of 500 με. It can be observed from the plot that the slope of unloading response is slightly higher than the loading; this resulted from a small amount of residual strain (about 25 με) left after the loading process. The strain transfer for the embedded sensor is 38%. The lower strain transfer will be discussed later in the section. For the non-embedded sensor, the strain was applied until the fusion joint broke loose from the cavity; it was verified under a microscope that the cavity broke at the fusion joint. The breaking point for the EFPI was observed to be at 3800 με, which is consistent with the strain limits of the fused silica optical fiber. The breaking point is marked with a red dashed-line.

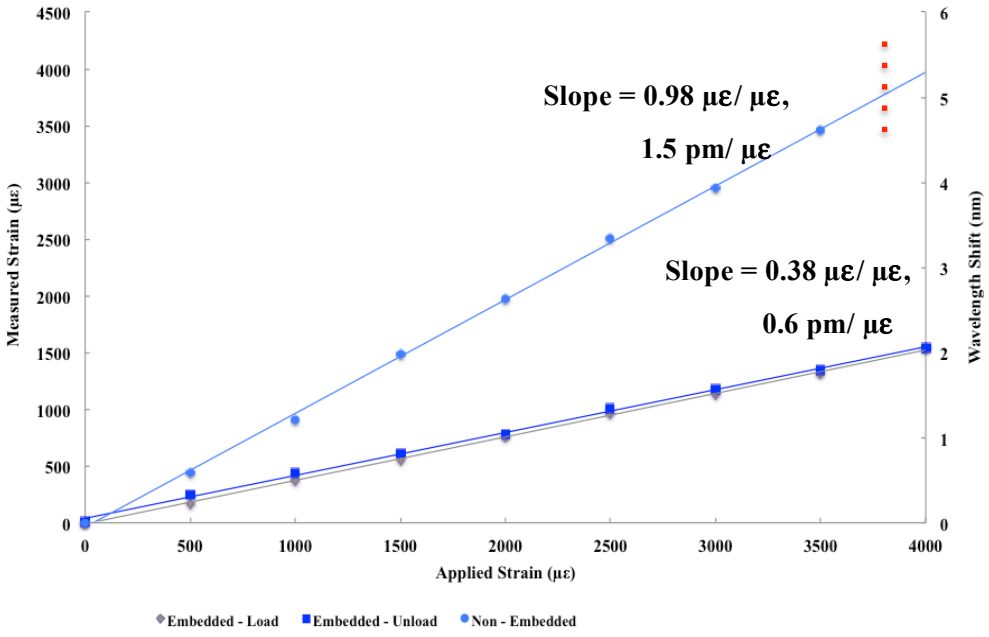

Figure 4.3 Measured strain response of the embedded and the non-embedded sensors at room temperature.

As discussed earlier in this section, the strain transfer ratio for the embedded sensor was about 38%. After investigating the potential reasons for the lower strain transfer, it was determined that the bond between the carbon fibers (comprising the laminate sheets) and the optical fiber sensor might not be very strong. To improve the strength of the bond between the carbon fibers and the optical fiber, the sample was cured further by keeping it at 200ºC for 3 hours and then, letting it cool down to room temperature (inside the furnace). This post-cured sample was then tested for its strain sensitivity. The post-cure temperature and time limits were followed as per the manufacturer's recommendations.

Figure 4.4 shows the comparison between the strain transfer of the pre-cure and the post-cure samples. It can be seen that the strain transfer improved immensely but there is an error in strain transfer. Instead of 100% transfer as in the case of non-embedded sensor, the embedded sensor detects an additional strain. The error increases with an increase in the applied strain. The error in the measured strain as opposed to the applied strain ranged from about 5% for 1500 με to about 28% for the applied strain of 4000 με. So the error is within an acceptable range if the applied strain is under 2000 με and this provides a working range for most applications.

There are various factors that might have contributed to this behavior including imperfect alignment of the laminate sheets during the manufacture process. Since the laminate sheets are aligned manually by stacking them on top of each other, human error contributes to the imperfection. Other types of composites have been known to carry large residual stresses and strains if subjected to elevated temperatures again after the first cure process during the manufacturing of the sample [51][52]. These residual stresses might have contributed towards the observed behavior. Since the error is consistent within a range and the results are linear, the measured strain can be calibrated easily. To further rectify this problem, certain recommendations regarding studying the effects of different combinations of cure time and temperature have been made in the future work section.

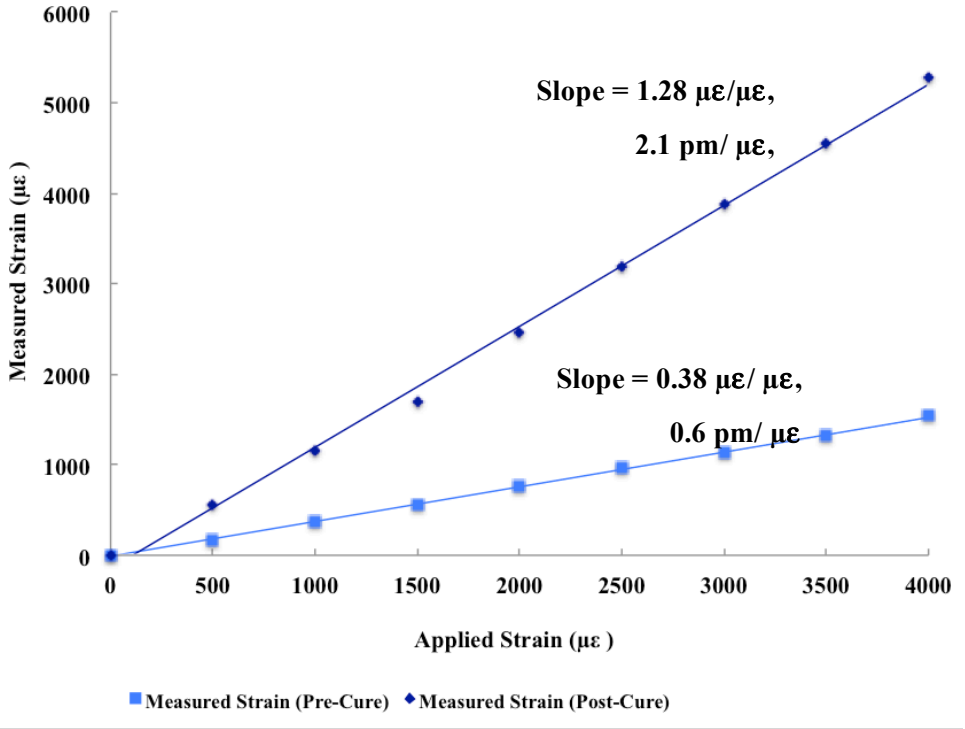

Figure 4.4 Measured strain response of the embedded sensor for pre-cure and post-cure processes.

The sensor was also used to observe its response towards the applied strain at temperatures above room temperature. The results are presented in Figure 4.5. The ambient temperature of 104.4 ºC yielded a response with a slightly higher slope. The primary reason behind this is the mismatch between the coefficient of thermal expansion values of the BMI matrix and the carbon fibers. This in turn results in the change of Tensile Modulus of the material leading to different strain transfer rates at different temperatures. Because of the low-sensitivity of the sensor towards the temperature, the difference in the slopes was only 0.1 pm/με. The temperature sensitivity is discussed in detail in the next section of this chapter.

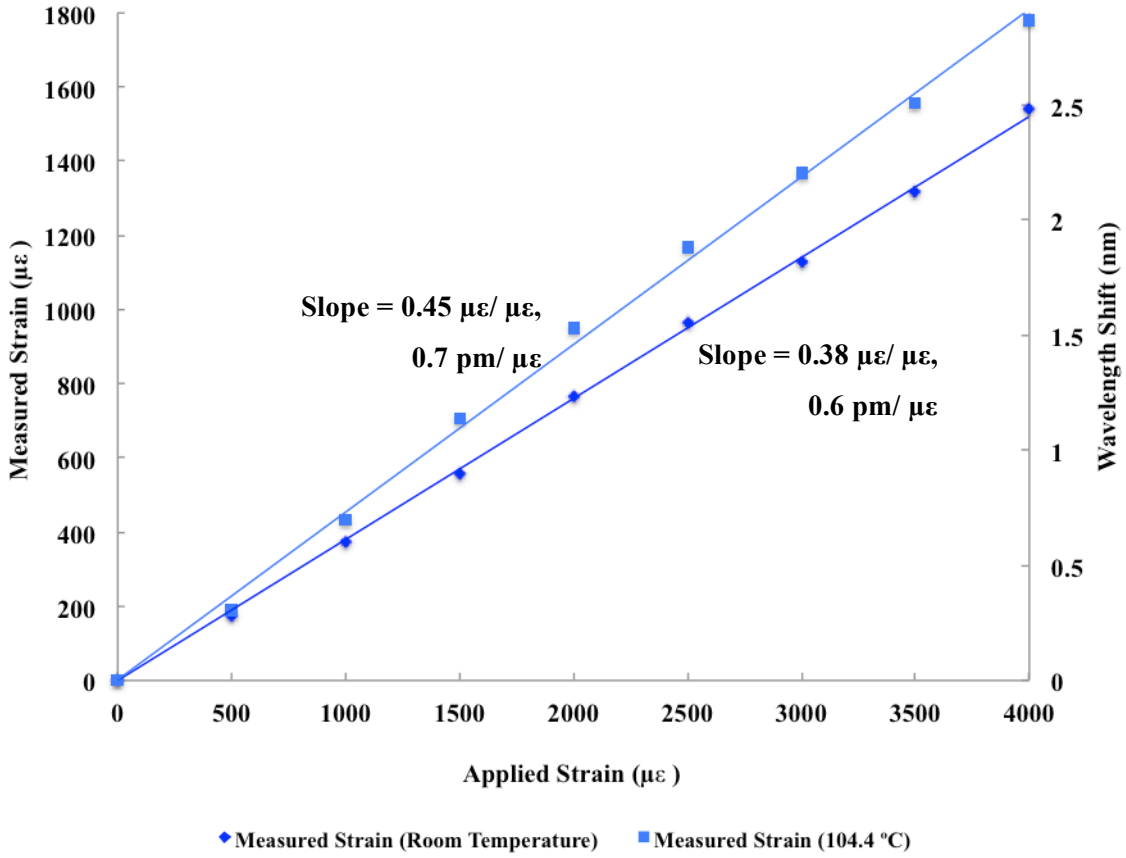

Figure 4.5 Measured strain response of the embedded sensor at room temperature and at 104.4 ºC.

4.2.2 IFPI Sensor. Strain sensitivity of the IFPI sensor is same as the EFPI sensor since their operational principle and dependence of wavelength change on the cavity length is the same. This was also verified by testing the IFPI sensor in non-embedded and embedded conditions by exerting axial strain on it. Strain sensitivity responses of the non-embedded and the embedded sensors at room temperature are presented in Figure 4.6. As can be observed from the plot, the embedded sensor has a lower slope (0.6 pm/με) as compared to the non-embedded sensor (1.4 pm/με) and the strain response is similar to the EFPI sensor. Strain transfer ratio for embedded sensor was calculated to be

38%. These sensitivity coefficients are same as the EFPI sensors except for a slight difference of 0.1 pm/με in case of the non-embedded sensor.

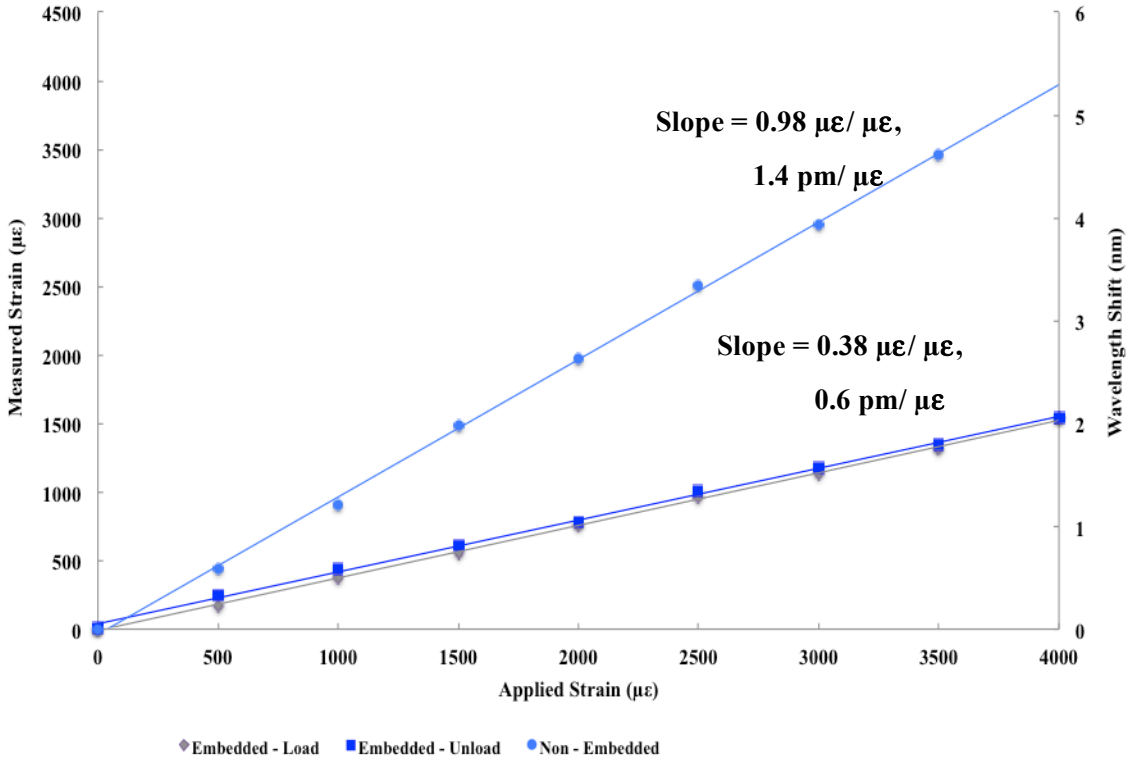

Figure 4.6 Measured strain response of the embedded and the non-embedded IFPI sensors at room temperature.

4.3 EXPERIMENTAL SET UP FOR TEMPERATURE SENSING

For the temperature testing, the sensor/embedded sample was placed inside a box furnace (Lindberg/Blue M). As seen in the Figure 4.7, the rest of the data acquisition set-up was the same as that of the strain sensing. The temperature of the furnace was raised

from 50 ºC to 800 ºC in steps of 50 ºC and the resultant wavelength shift in the spectrum was recorded using the OSA.

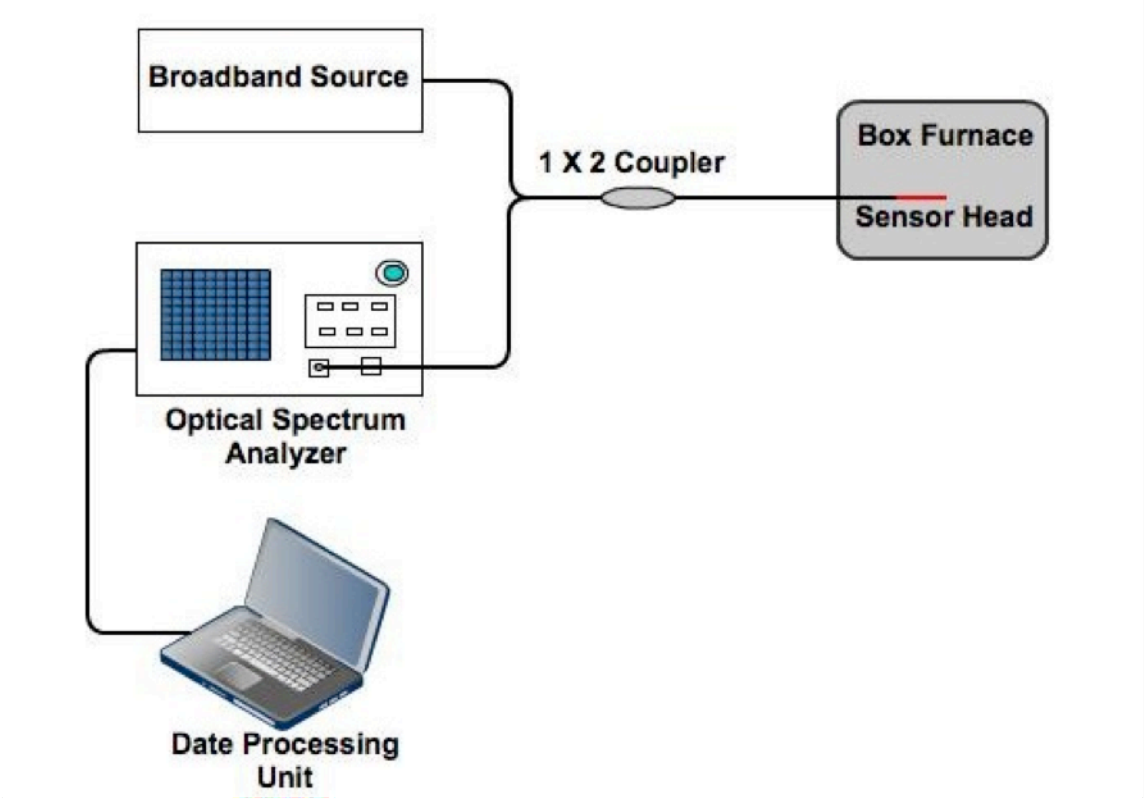

Figure 4.7 Experimental set up for temperature testing of embedded and non-embedded sensors

4.4 EXPERIMENTAL RESULTS FOR TEMPERATURE SENSING

In this section, the experimental results for temperature testing on EFPI and IFPI sensors are presented and discussed.

4.4.1 EFPI Sensor. Figure 4.8 shows the wavelength shift resulting from the increasing ambient temperature as observed by using the non-embedded and embedded

EFPI sensor. The slope of the response was calculated to be 0.59 pm/ºC for the non-embedded sensor and the coefficient of thermal expansion (CTE) of silica was calculated (from the acquired data) to be 0.715 x 10^{-6}/ºC, which is 1.3 times larger than that of the actual CTE (0.55 x 10^{-6}) [50]. Temperature response of the sensor embedded in carbon composite laminates is also presented. The slope and CTE calculated from the sensor response were 1.742 pm/ºC and 1.615 X 10^{-6} /ºC, respectively. The CTE of the BMI resin using the embedded sensor was 1.615 x 10^{-6}/ºC which is smaller than the actual value of the resin that ranges from 24 x 10^{-6} /ºC to 44 x 10^{-6} /ºC but about 2.3 times larger than the

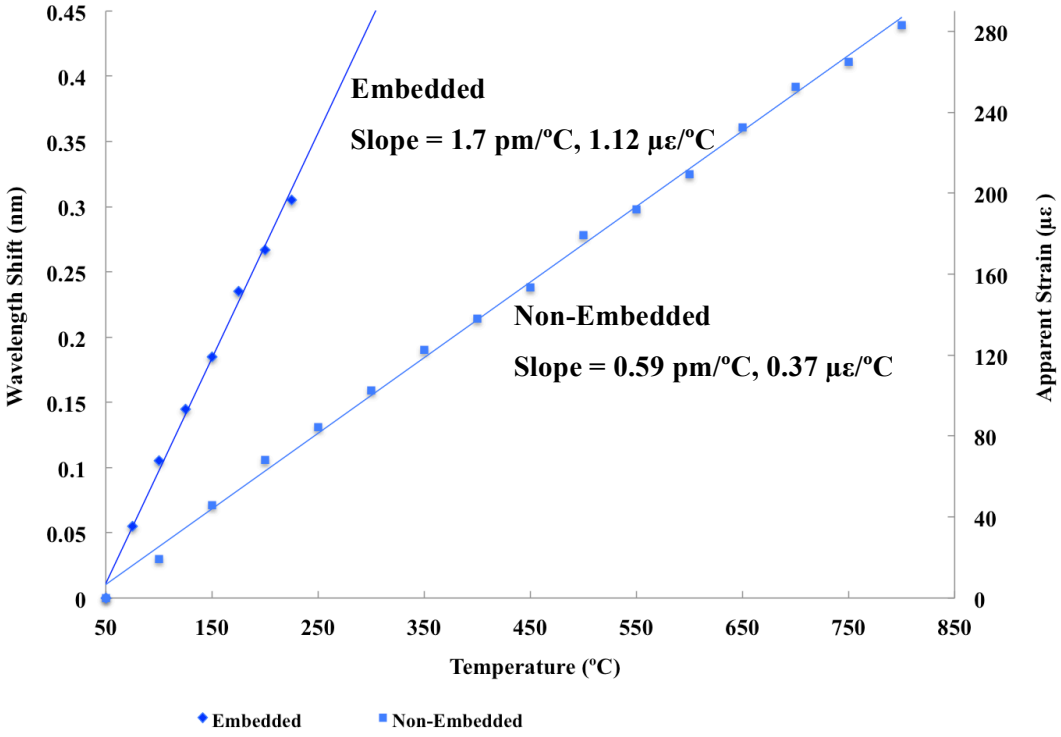

Figure 4.8 Results for temperature testing of embedded and non-embedded EFPI sensor

calculated CTE of silica [42]. The apparent strain is also shown on the secondary axis in the Figure 4.8. For the non-embedded sensor, the calculated strain resulting from the cavity expansion was 0.37 με/ºC whereas the strain exerted for embedded sensor was calculated to be 1.12 με/ºC. Larger strain in case of embedded sensor might have resulted from the strain exerted on the sensor by the surrounding composite laminates. The sensor is not very sensitive towards the temperature, but it does respond very well towards the thermal strain of the host structure.

The sensor's capability for handling high temperatures was also tested by keeping it at 650 ºC for 3 hours. No change in the reflection spectrum was observed and the sensor survived the whole process without any deterioration in performance.

4.4.2 IFPI Sensor. As mentioned before, the IFPI sensor is known to have higher temperature sensitivity as compared to an EFPI sensor. Figure 4.9 shows the data comparing the two sensitivities for the sensors in the non-embedded state. The corresponding slopes obtained were 0.59 pm/ºC and 14.9 pm/ºC for EFPI and IFPI, respectively. It can be concluded from the data obtained that the temperature sensitivity of the IFPI sensor is about 25 times that of the EFPI sensor.

Figure 4.10 shows the comparison of the temperature responses for the embedded and the non-embedded EFPI sensors. The slightly higher slope of the embedded sensor might have resulted from the strain exerted on the sensor by the surrounding composite laminates due to a CTE mismatch between the BMI matrix and carbon fibers (comprising the BMI material). The sensor is sensitive to both the temperature and the strain.

4.5 CURE MONITORING SET UP AND RESULTS

The EFPI sensor was used for the cure monitoring of BMI during the sample manufacturing process. In-situ monitoring of the samples was performed by recording the spectra of the EFPI sensor during the process of embedding the sensor in BMI. Figure 4.11 shows the results obtained and various stages of the curing process are marked. The curing takes place in two steps. First, the prepreg layup is heated to 250 ºF for 1 hour. In the end of this stage, the viscosity of the resin increases. Then, it is heated to 375ºF for two hours.

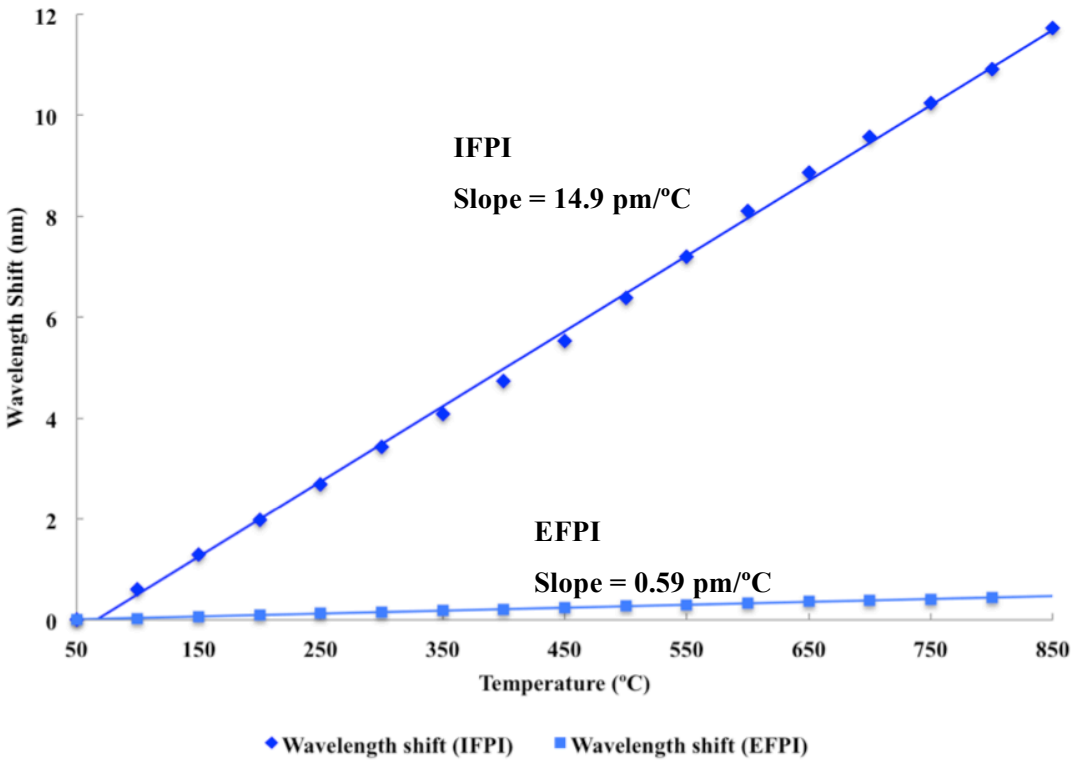

Figure 4.9 Comparison of the temperature sensitivities of the non-embedded EFPI and IFPI sensors

At this point, the resin begins to cure. As the glass transition temperature of the system approaches its cure temperature, the vitrification stage begins. As the degree of cure of the system increases (uncured prepreg to a cured composite), the glass transition temperature (T_g) of the system also improves. At one point the T_g is equal to the cure temperature (temperature of the oven). This marks the beginning of vitrification process where the system begins to transform from a rubbery viscoelastic material to a brittle glassy material. After vitrification, the rate of cure also reduces because of reduced mobility of polymer chains. The curve plotted below matches the actual cure cycle of BMI well.

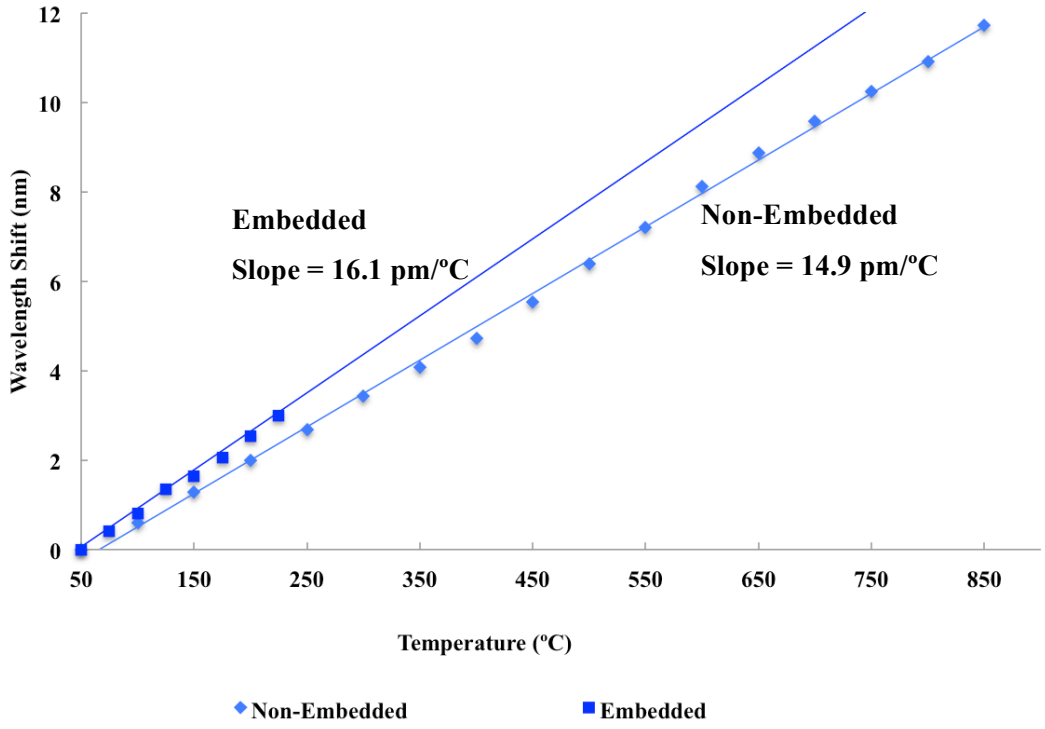

Figure 4.10 Results for temperature testing of embedded and non-embedded IFPI sensor

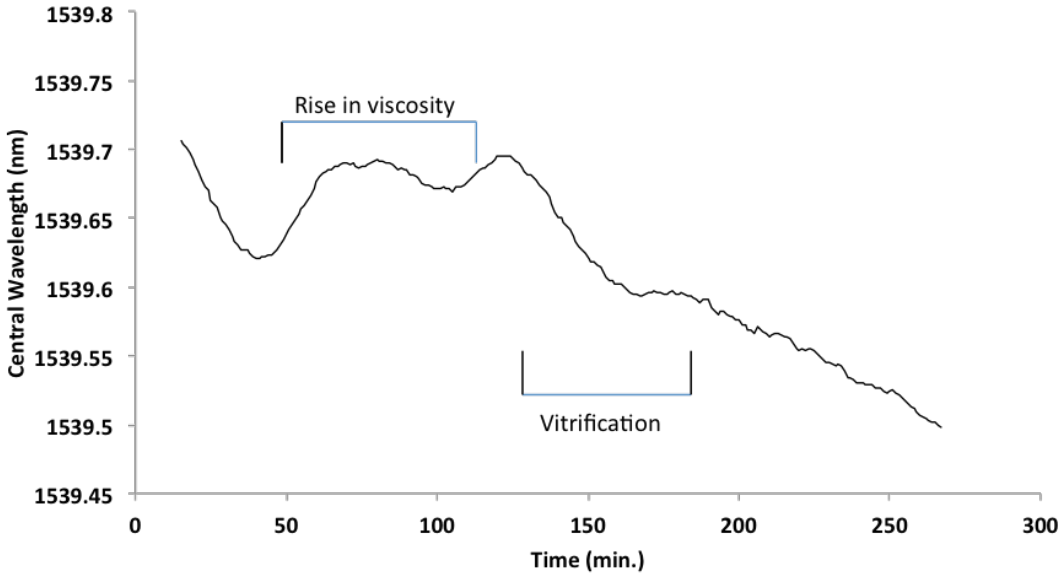

Figure 4.11 Results for cure monitoring of BMI sample using EFPI sensor

4.6 CONCLUSIONS

Experimental procedures used to investigate and demonstrate the sensor applications were discussed in this section. Results obtained from the experiments conducted were also presented and discussed. From the results obtained, it can be concluded that the EFPI sensor is more suitable for the strain monitoring applications where the ambient temperature may be higher than room temperature because of the negligible dependence of its wavelength change on the ambient temperature. Both EFPI and IFPI sensors respond the same towards exerted strain but the IFPI sensor is about 25 times more sensitive to the ambient temperature. Table 4.1 lists the strain and temperature ranges over which both EFPI and IFPI sensors were tested in non-embedded and embedded conditions. In addition to the strain and temperature monitoring applications, the EFPI sensor was also used for cure monitoring of the BMI.

Table 4.1 Testing parameters for embedded and non-embedded sensors.

Sensor	**Testing Parameter**	**Lower Limit Tested**	**Upper Limit Tested**	**Response Factor**
Non Embedded	Temperature	50 ºC	800 ºC	Wavelength Shift
Embedded	Temperature	50 ºC	225 ºC	Wavelength Shift
Non Embedded	Strain	0 με	3700 με	Wavelength Shift
Embedded	Strain	0 με	4000 με	Wavelength Shift

5. SIMULTANEOUS MEASUREMENT OF STRAIN AND TEMPERATURE

A hybrid sensor design based on combining the EFPI and IFPI sensors is proposed in this section. This design is intended for simultaneous measurement/monitoring of both strain and temperature in embedded as well as non-embedded applications. The design and fabrication of the sensors, experiments conducted, results obtained and signal-processing methods used have been presented and discussed.

5.1 BACKGROUND

Simultaneous measurement of strain and temperature is very helpful in the fields of structural health monitoring. Different sensing techniques have been used in recent years for the purpose. One of the very common sensing devices used is the long-period fiber grating (LPFG) or fiber Bragg-gratings for their inherent sensitivity towards both strain and temperature. In the past, a dual-LPFG structure has been employed where one of the gratings exhibits a positive temperature sensitivity whereas the other exhibits a negative temperature sensitivity. The LPFGs are combined separating the sensitivity peaks in the spectra at a desirable length [53]. Dual FBGs have also been used in a similar structure for simultaneous measurement of temperature and strain [54]. Another method uses a sensor with fiber Bragg grating comprising the sensing-end and a multimode fiber section is used at the other end [55]. Other methods include using a combination of fiber gratings and interferometers [56].

Using a combination of sensors one each for measuring temperature and strain allows for better calibration but makes it difficult to extract the data pertaining to individual parameters. Length of the sensors might not be ideal for embeddable applications, especially if the fiber gratings are involved since these are on the order of a few centimeters and additional separation distance between two gratings will add to the length. Demonstrated in the following sections is a hybrid sensor using two types of interferometers, extrinsic and intrinsic, combined for simultaneous measurement of strain

and temperature. The EFPI sensor is used for calibrating the strain as it is temperature insensitive and both EFPI and IFPI sensors have same strain sensitivity. The sensor is easy to use for embeddable applications due to the compact sizes of these interferometers.

5.2 SENSOR FABRICATION

Figure 5.1(a) shows the schematic diagram of the hybrid sensor. The hybrid sensor was fabricated by cascading the EFPI and the IFPI sensors. EFPI and IFPI sensors were fabricated using the same process as described in Section 3. The fs-laser micromachining was used to fabricate both of the devices. A micro-cavity was created on a SMF end-face and then fused with another piece of SMF to fabricate the EFPI sensor whereas to fabricate the IFPI, two microstructures were created inside the SMF on its core. A micro-cavity created on a SMF end-face and then fused with the IFPI also results in the same structure. Since the optical fiber has a very low loss, both of the methods yield similar results in terms of reflection spectra. Figures 5.1 (b) and (c) show the microscopic views of the IFPI and the EFPI respectively. After fabricating the EFPI and IFPI sensors separately, they were fusion spliced together at a desired separation distance. The separation distance was determined by the quality of the hybrid reflection spectrum, the distance that yielded the highest quality but maintained a manageable sensor length was used. The separation distance varies with the sensor quality but it is approximately a couple of centimeters.

The reflectivity of the air/glass interfaces in the EFPI is much larger than the reflectivity of the glass reflectors created on the core of the IFPI. This results from a very small refractive index change (10^{-4}–10^{-2}) induced by the fs-laser fabrication of the micro-reflectors on the SMF core to fabricate IFPI sensor [56]. This mismatch in the reflectivity results in a mismatch of power levels observed on the EFPI and the IFPI spectra. To improve the power levels and the quality of the hybrid spectrum, a CO_2 laser was used to add transmission loss to reduce the reflectivity of the EFPI as described in [57]. A SYNRAD, Inc. CO_2 laser with a free space wavelength of 10.6 μm was used to increase the loss by producing regions of slightly different refractive index. Focusing the laser and heating the fiber region between the IFPI and EFPI devices achieved this. The laser

output power and the irradiation time were computer controlled and in-situ monitoring of the hybrid spectrum was done in order to generate an appropriate loss. In addition to the transmission loss, the EFPI was used at the far end of the sensor while connecting the IFPI end to the measurement system while using the sensor in the experiments.

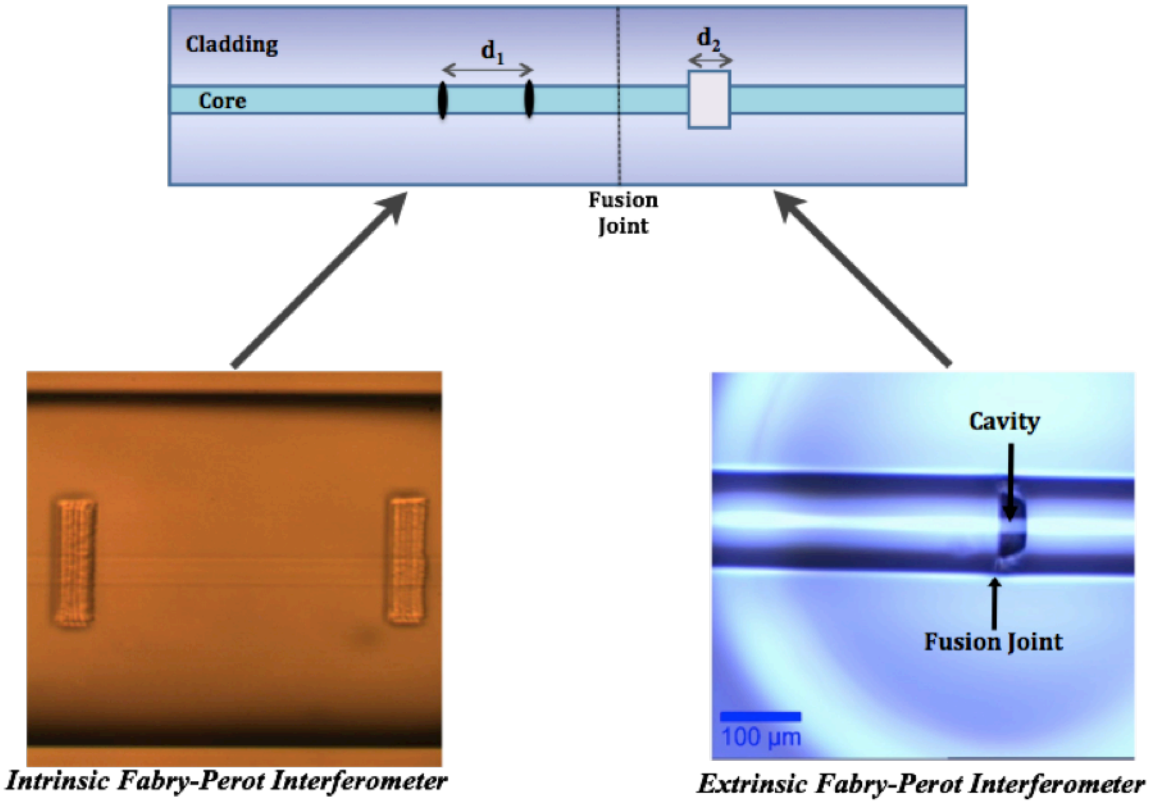

Figure 5.1 Images of the hybird sensor. (a) Schematic diagram of the hybrid sensor. (b) Microscopic image of the IFPI sensor. (c) Microscopic image of the EFPI sensor.

5.3 OPERATIONAL PRINCIPLE

As discussed and demonstrated in Section 4 of this dissertation, strain sensitivity of both EFPI and IFPI sensors is same but the IFPI sensor is almost 25 times more

sensitive towards the ambient temperature changes as compared to the sensitivity of EFPI. This results in a unique opportunity of combining the two sensors for the simultaneous measurement of strain and temperature. Since the temperature dependence of the EFPI sensor is negligible, this micro-cavity sensor was used for calibration of the strain reading whereas the IFPI sensor was used to monitor the sensor response resulting from the temperature changes.

A sensitivity matrix was used to extract the strain and temperature components based on the individual sensitivity coefficients of the EFPI and the IFPI sensors. Following are the equations that form the sensitivity matrix. Dependence of the wavelength shift in the spectrum of EFPI and IFPI on changes in strain and temperature can be described as:

$$\Delta\lambda_E = K_{\varepsilon,E}.\Delta\varepsilon + K_{T,E}.\Delta T \tag{5.1}$$

$$\Delta\lambda_I = K_{\varepsilon,I}.\Delta\varepsilon + K_{T,I}.\Delta T \tag{5.2}$$

Subscripts E and I are used for the terms corresponding to the EFPI and IFPI sensors, respectively. Subscripts ε and T represent the strain and temperature contributions, respectively. λ is the wavelength, Δ represents a change in the associated quantity and K is the sensitivity coefficient for the associated quantity. Equations 5.1 and 5.2 can be represented using a matrix solution as following:

$$\begin{bmatrix}\Delta\lambda_E \\ \Delta\lambda_I\end{bmatrix} = \begin{bmatrix}K_{\varepsilon,E} & K_{T,E} \\ K_{\varepsilon,I} & K_{T,I}\end{bmatrix}\begin{bmatrix}\Delta\varepsilon \\ \Delta T\end{bmatrix} \tag{5.3}$$

The matrix equation 5.3 can be solved to find the strain and temperature components as follows:

$$\begin{bmatrix}\Delta\varepsilon \\ \Delta T\end{bmatrix} = {}^{1}/_{K}\begin{bmatrix}K_{T,I} & -K_{T,E} \\ -K_{\varepsilon,I} & K_{\varepsilon,E}\end{bmatrix}\begin{bmatrix}\Delta\lambda_E \\ \Delta\lambda_I\end{bmatrix} \tag{5.4}$$

$K = K_{\varepsilon,E}.K_{T,I} + K_{T,E}.K_{\varepsilon,I}$ in the above equation.

5.4 SIGNAL PROCESSING

Since the resultant reflection spectrum of the hybrid spectrum consists of both the EFPI and IFPI spectra, signal processing is required to extract the individual components. The demodulation technique used for the work presented here is similar to the one used

by Wenyuan Wang et al. [58]. Figure 5.2 shows different steps involved in the signal processing. The spectrum is first converted from the wavelength domain (or axis) to the wavenumber domain (or axis). This conversion makes it easier to apply the Fast Fourier Transforms or FFT in step 2. Hamming window filters are then applied to filter the desired frequency components to be considered. The components are the individual components corresponding to the EFPI and the IFPI spectrum. The inverse FFT is applied to the extracted frequency components to reconstruct the EFPI and IFPI spectra.

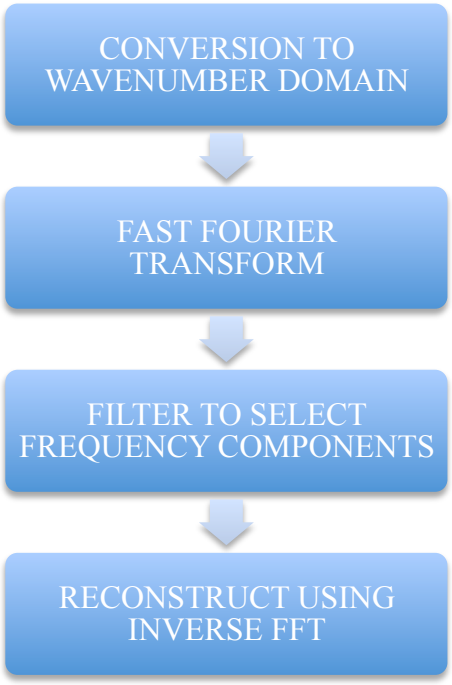

Figure 5.2 Different steps involved in the signal processing of the hybrid sensor spectra

Figure 5.3 shows the reflection spectrum of the hybrid sensor. Smaller frequency changes represent the EFPI component whereas larger frequency components are the spectral contributions of the EFPI sensor. Figure 5.4 shows the results obtained after step

2, i.e. after applying the Fast Fourier Transforms to the hybrid spectrum. The individual components of the EFPI and the IFPI sensors can be observed. Hamming window filters are then applied to select individual frequency components [59]. These filters result in the extracted individual frequency components. The inverse FFT is then applied to reconstruct the spectra corresponding to the EFPI and the IFPI sensors. Figures 5.5 and 5.6 show the reconstructed spectra corresponding to EFPI and IFPI using the inverse FFT, respectively.

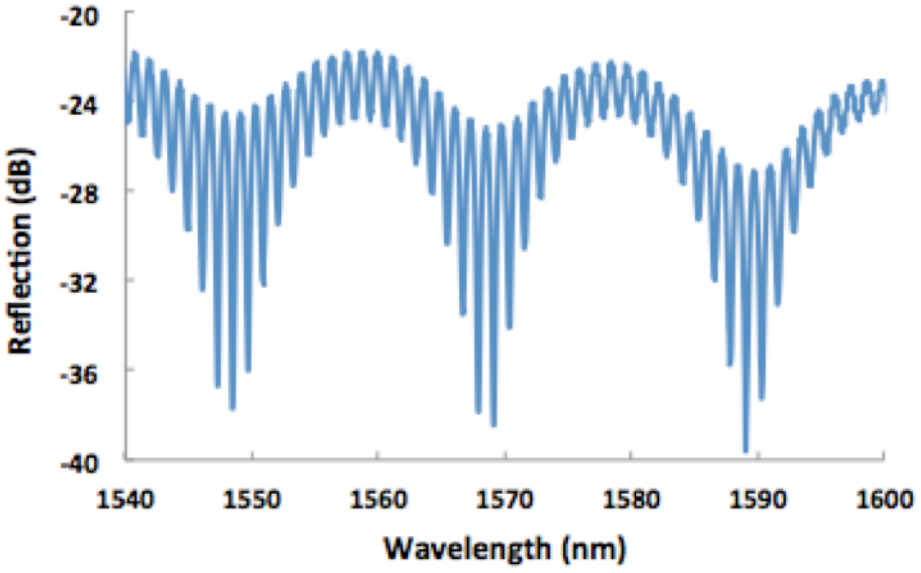

Figure 5.3 Reflection spectrum of the hybrid sensor consisting of EFPI and IFPI components.

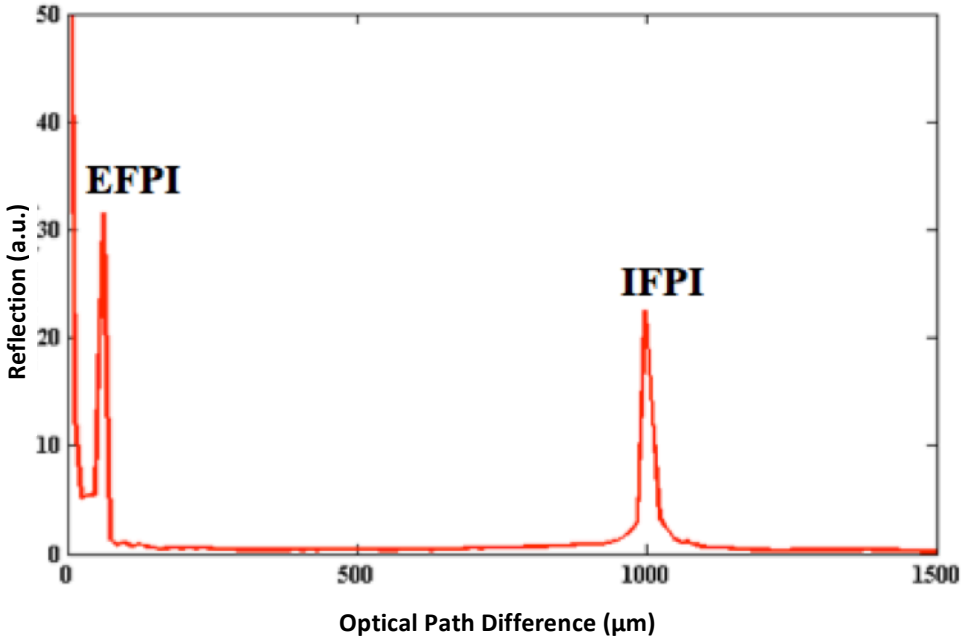

Figure 5.4 FFT signal of the hybrid sensor separating EFPI and IFPI signals

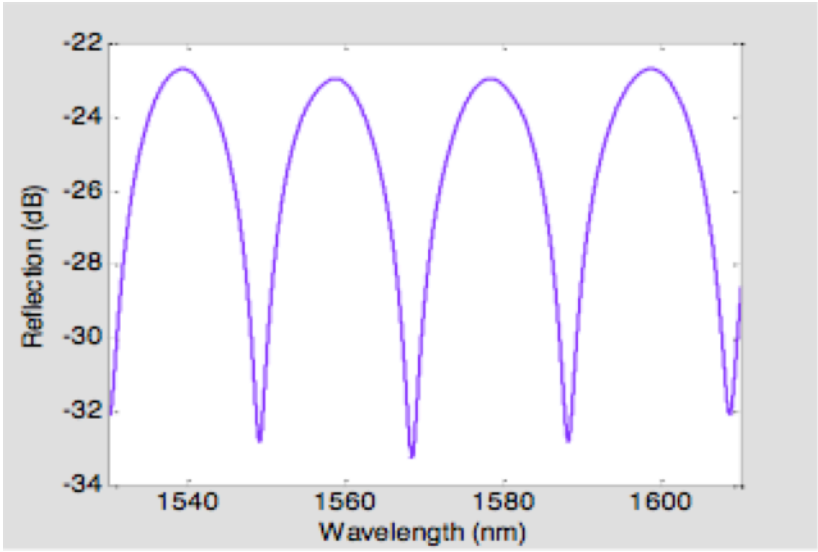

Figure 5.5 Reconstructed spectrum of the EFPI sensor using Inverse FFT.

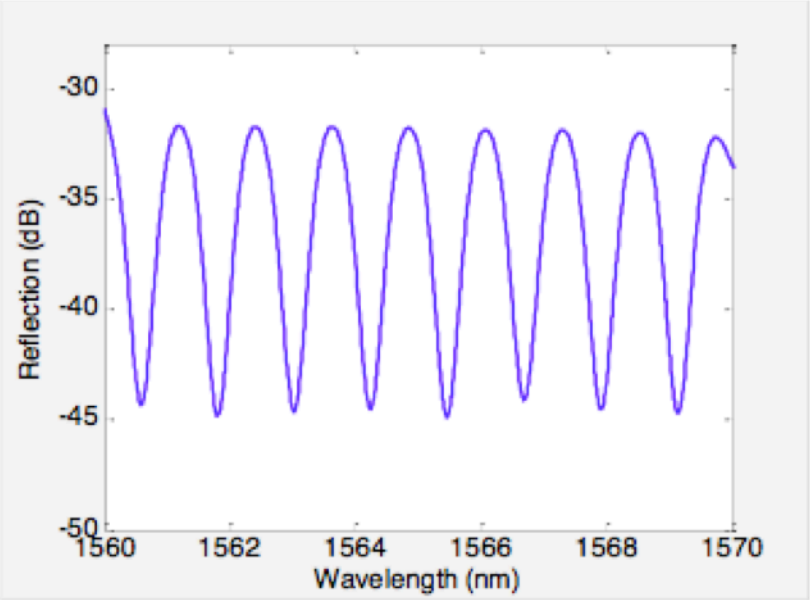

Figure 5.6 Reconstructed spectrum of the IFPI sensor using Inverse FFT.

5.5 EXPERIMENTAL SET UP

For simultaneous application of temperature and strain on embedded sensors, a movable furnace capable of encasing the strain applicator grips inside it was used. Figure 5.7 shows the furnace with the grips already positioned inside it. Thermal wool was used to fill in any gaps around the grip openings to insulate the furnace properly. The sample with embedded sensor can also be seen placed inside the furnace before mounting it on the grips. A fixed temperature was used while the strain was varied for this experiment. The sample was placed inside the furnace while the temperature reached a desired level so that the sample temperature would closely match the temperature of the furnace.

Figure 5.7 The strain frame encased inside the furnace for simultaneous application of temperature and strain.

Figure 5.8 below shows a complete setup where the BMI sample with the embedded sensor has already been installed inside the furnace and the sensor is connected to the power source and the OSA using a 1 x 2 coupler for in-situ monitoring of the spectra. The collected spectra were then analyzed for the wavelength shift (by using the first collected spectrum as reference). The sample was kept inside the furnace at room temperature and was allowed to heat as the furnace acquired a desired testing temperature.

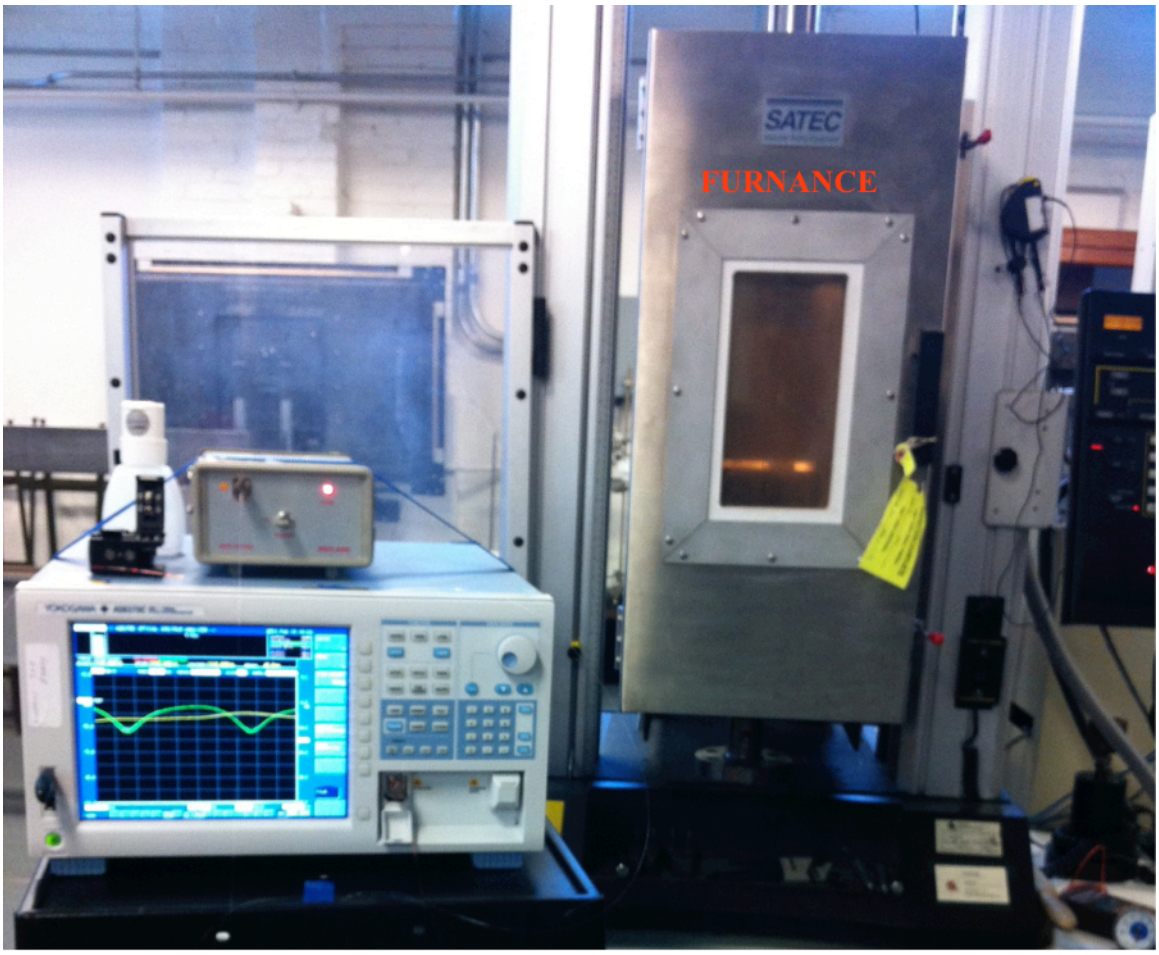

Figure 5.8 Experimental set up for the simultaneous testing.

5.5.1 Challenges Involved with Using Hybrid Sensor for Embeddable Applications. Though potential of simultaneous measurement offers a great opportunity for smart structure monitoring, there are some challenges that should be taken into account. These are listed as follows:

- If length of the sensor is longer than a few centimeters, it is difficult to prepare the embedded sensor sample. Most of the in-lab testing is done on smaller samples and a longer sensor prohibits the flexibility of installment.
- The sensor needs to be routed out of the side of the sample instead of the ends coming out of the top and bottom of the sensor. This is to avoid

damaging the sensor while installing the sample on the grips of the strain frame. This prohibits the use of the full length of the sample for embedding the sensor.

- If the sensor end-face is embedded inside the sample, unintended noise might result during the curing process as the resin coagulates around the sensor. This problem can be easily fixed by leaving the fiber end-face out of the sample; this will allow for a better control of eliminating the noise. The reflections from the fiber end-face can be eliminated by roughening the surface and making it uneven using the fs-laser. A refractive index matching liquid can also be used to eliminate any unintentional reflections from the fiber end-face.

5.5.2 Experimental Results. Substituting the sensitivity coefficients in Equation 5.4 with the coefficients calculated in Section 4, the following equations can be used for computing individual strain and temperature components. The data corresponding to these coefficients was presented in Section 4 in Figures 4.5, 4.7, 4.8 and 4.10. Table 5.1 summarizes various coefficient values computed. K is the sensitivity coefficient, subscripts E and I represent the values corresponding to the EFPI and IFPI sensors, respectively and subscripts ε and T represent the strain and temperature sensitivities, respectively.

Table 5.1 Sensitivity coefficients for embedded and non-embedded testing.

Coefficients →	$K_{\varepsilon,E}$	$K_{\varepsilon,I}$	$K_{T,E}$	$K_{T,I}$
Non-Embedded	1.5 pm/με	1.4 pm/με	0.6 pm/ºC	14.9 pm/ºC
Embedded	0.6 pm/με	0.6 pm/με	1.7 pm/ºC	16.1 pm/ºC

Equation 5.5 is for the non-embedded testing and equation 5.6 is for the embedded testing parameters. K is a constant calculated individually for embedded and

non-embedded equations, Δλ is the wavelength shift; ΔT and Δε are the temperature and strain changes, respectively. Subscripts E and I represent the values pertaining to the EFPI and IFPI calibrations. Wavelength shift is measured in pm, temperature in ºC and the strain in με.

$$\begin{bmatrix}\Delta\varepsilon\\ \Delta T\end{bmatrix} = {}^{1}/_{K}\begin{bmatrix}14.9 & -0.6\\ -1.4 & 1.5\end{bmatrix}\begin{bmatrix}\Delta\lambda_E\\ \Delta\lambda_I\end{bmatrix}\ , K = 21.51 \tag{5.5}$$

$$\begin{bmatrix}\Delta\varepsilon\\ \Delta T\end{bmatrix} = {}^{1}/_{K}\begin{bmatrix}16.1 & -1.7\\ -0.6 & 0.6\end{bmatrix}\begin{bmatrix}\Delta\lambda_E\\ \Delta\lambda_I\end{bmatrix}\ , K = 8.64 \tag{5.6}$$

Figure 5.9 shows the data plotted for the experiment where the temperature was kept at 104 ºC and the strain was varied from 0 – 1500 με in steps of 250 με. As can be observed from the plotted data, the calculated strain matched well with the measured strain. Calculated strain refers to the strain calculated using the sensitivity matrix. Measured strain is based on the data collected using EFPI sensor only. As discussed in the Section 4, strain transfer was about 38% of the applied strain. The calculated strain is within the transfer ratio displayed for individual EFPI and IFPI sensors in embedded conditions.

5.6 CONCLUSIONS

A potentially useful hybrid sensor design based on EFPI and IFPI sensors was discussed in this section. Using appropriate signal modulation techniques, this sensor can be used for simultaneous measurement of the strain and temperature. EFPI sensor is used to calibrate for strain since the temperature interference on the wavelength shift for the EFPI sensor is minimal. Signal demodulation method based on Fast Fourier Transform was also presented and discussed. Experimental set up for the application of strain and elevated temperatures was also discussed. Challenges faced during the testing of embedded hybrid sensor were also discussed. In conclusion, hybrid sensor was successfully demonstrated for the non-embedded applications but in-depth investigation is needed on how to successfully use the sensor for embeddable application without incurring unintended loss in the reflection spectrum.

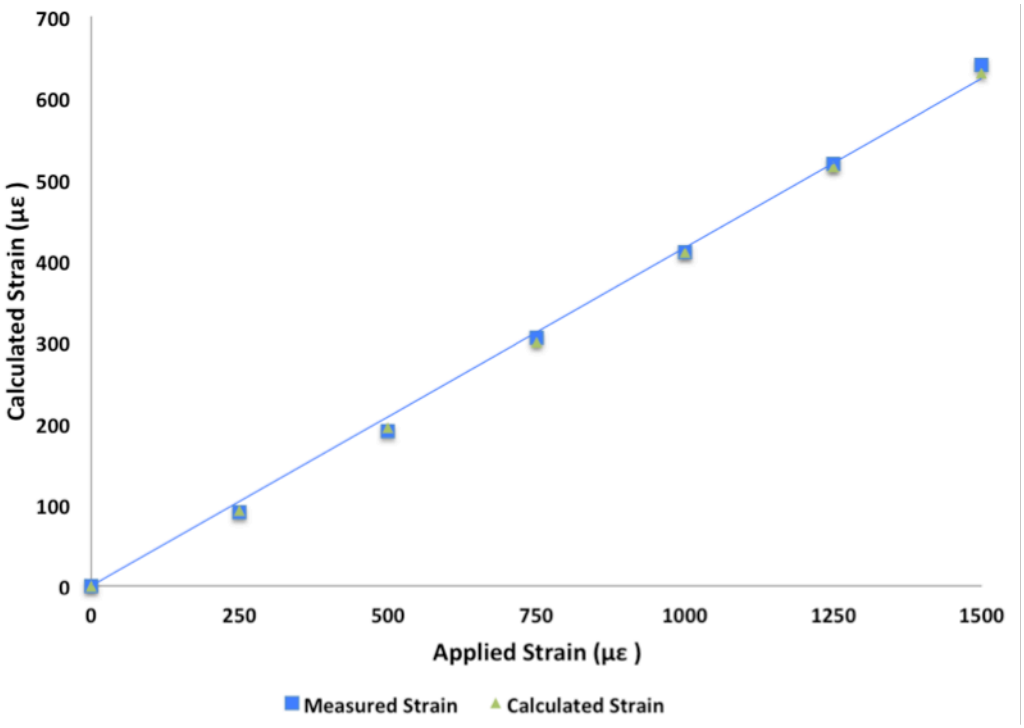

Figure 5.9 Measured and calculated strain for non-embedded hybrid sensor at 104 ºC.

6. SUMMARY AND FUTURE WORK

This section summarizes the work presented in the dissertation. The background on which the research is based, the fabrication process and operational principles of the sensors, experimental results, and contributions made by this research work are discussed in this section. Apart from summarizing the work, the recommended future work is also included.

6.1 SUMMARY OF THE WORK PRESENTED IN THE DISSERTATION

Miniaturized sensors that are easy to handle are highly sought after in the industry where in-situ monitoring is required in harsh environments. These harsh environments may be due to corrosive atmosphere, high temperatures, high pressure, and presence of strong electromagnetic interference (EMI) noise. Along with the harsh environment requirements, aerospace and mechanical applications like structural health monitoring demand sensors that are embeddable. Sensors currently available may meet one or two of the conditions but not all of them. This suggests a gap that needed to be filled with innovative research.

Due to their compact size, immunity from electromagnetic interference, high temperature tolerance, immunity to EMI, low loss over long distance interrogation and capability of multiplexing, optical fiber based sensors have been used for sensing and monitoring applications. But there exist a number of issues including cumbersome designs, temperature cross-sensitivity, and multiple components comprising the sensor, etc., with the already available sensors in the market. These factors either contribute to a large error in the data or make it very difficult for the sensors to be used in any type of embeddable applications.

Motivated by the existing limitations and need for better sensors for harsh environments and structural health monitoring applications, the work presented in this dissertation was focused on the design, fabrication and demonstration of small-sized optical fiber sensors for embeddable applications. To meet the objectives, two basic

optical fiber sensor designs were explored that were fabricated using a laboratory integrated femto-second laser micromachining system. For the extrinsic Fabry-Perot interferometer (EFPI) design, the fs-laser was used to ablate and remove the material off the fiber end face while for intrinsic Fabry-Perot interferometer (IFPI) design, the laser power was focused inside the fiber on the fiber core to create two microstructures.

The sensors used for the work reported in this dissertation survived a high temperature of 850 ºC. These sensors were tested for their embedded responses by embedding them inside carbon composite based Bismaleimide (BMI) laminates. High performance carbon composites are used in aerospace applications as they provide good mechanical performance at elevated temperatures. The sensor to be tested was placed in between the middle layers of a six-layer unidirectional laminate. The laminates were fabricated using IM7G/AR4550 prepreg by out-of-autoclave process. The embedded sensors were used for strain, temperature and cure monitoring of the BMI laminates.

The first optical fiber sensor was based on the EFPI design and was aimed at strain monitoring applications at elevated temperature. The sensor was fabricated using the fs-laser system by creating a micro-cavity on the fiber end face and fusing another part of the fiber to the cavity thus creating an air cavity encapsulated inside the fiber. The silica material of the optical fiber sensor and the thermal stability resulting from the fs-laser fabrication enables the sensor to withstand very high temperatures. At the same time, a single fusion joint allows for better structural integrity and ease-of-fabrication over tube-encapsulated designs. The inherent properties of the fused silica and the EFPI cavity structure enable the sensor to be used as an efficient strain sensor. For the non-embedded sensor, the temperature sensitivity was calculated to be 0.59 pm/ºC and the coefficient of thermal expansion (CTE) of silica was calculated to be 0.715×10^{-6}/ºC. The temperature sensitivity and the CTE calculated for the embedded sensor were 1.742 pm/ºC and 1.615×10^{-6} /ºC, respectively. The strain sensitivities for the non-embedded and the embedded EFPI sensor were observed to be 1.5 pm/με and 0.6 pm/με, respectively.

The second optical fiber sensor was based on the IFPI design and was fabricated using fs-laser to create two microstructures (points or lines) on the core of the fiber inside the fiber. These structures were aligned to each other to form an interferometer. The IFPI

sensors are inherently sensitive towards strain as well as temperature but due to the temperature cross-sensitivity issue, this sensor was intended only for room temperature strain sensing applications. Since the sensor consists of silica material only and has no joints, its rugged design presents an apt opportunity for use in embeddable applications. The temperature sensitivity for the non-embedded IFPI sensor was 14.9 pm/ºC whereas for the embedded sensor, it was 16.1 pm/ºC. The IFPI sensor was about 25 times more sensitive towards temperature as compared to the EFPI sensor. The strain sensitivities for the non-embedded and the embedded IFPI sensor were observed to be 0.6 pm/με and 1.4 pm/με, respectively that are very close to the strain sensitivities of the EFPI sensor.

The abovementioned EFPI and IFPI sensors were combined by fusing them together at an appropriate distance for the third design to be used for applications where temperature as well as strain are required to be monitored simultaneously. A sensitivity matrix was used to extract the temperature and strain components. This hybrid sensor was then tested for its strain response at an elevated temperature. Since both EFPI and the IFPI sensors have same strain sensitivities but different temperature sensitivities, the EFPI sensor was used as a reference while using the hybrid sensor.

6.2 INNOVATIONS AND CONTRIBUTIONS

Major scientific and technical contributions of this work include the following.

- A new type of embeddable Extrinsic Fabry-Perot Interferometer sensor using fs-laser micromachining was fabricated. This sensor was fabricated for applications requiring embeddable strain sensors with minimal temperature interference. The micro-cavity based EFPI sensor demonstrated temperature insensitive strain sensing.
- A hybrid sensor using the EFPI and IFPI was fabricated for the simultaneous measurement of temperature and strain. The temperature and strain components were extracted using a simple sensitivity matrix. This sensor was fabricated for strain sensing applications at elevated temperatures requiring embeddable sensors. With many unique advantages such as linear response towards strain and temperature, small size, immunity towards electromagnetic interference,

flexibility of fabrication, ease of handling, high temperature survivability, usability in corrosive environment, and low loss over long distance data transfer operations, these sensors can be used for many embedded as well as non-embedded applications.

- Embeddability of both the EFPI and hybrid sensors was demonstrated using carbon fiber/ Bismaleimide (BMI) polymer by embedding the sensors in between the middle layers of the BMI laminates before the curing process. All of the sensors survived the curing process. BMI is a relatively new material and any research aimed at providing more data about the material response is highly desirable.
- For the first time, the strain characteristics of the carbon fiber/Bismaleimide (BMI) polymer were observed using the optical fiber sensors. The BMI composites are highly sought after for their flexibility and high strength. These composites are under investigation for their feasibility in aerospace applications, specifically for their usage in manufacturing airplane wings to study the dynamics of air pressure and temperature changes exerted on the wings during takeoff and landing procedures.
- The curing properties of the BMI polymer were also studied using the optical fiber EFPI sensors. The in-situ monitoring was performed during the sample manufacturing process. The characteristics obtained by analyzing the data obtained using the EFPI sensors produced results very similar to the expected theoretical curing cycle of BMI.

6.3 FUTURE WORK

The future work recommendations for sensor applications as well as sensor design and performance investigations are listed below.

- The micro-cavity EFPI sensors may be used to calculate the Poisson's Ratio by embedding them in a BMI composite along the 0º and 90º orientations to observe the strain exerted along both the x and y axes.

- The micro-cavity EFPI sensor and the IFPI sensor can be used for impact testing and strain profiling of the BMI composite samples. Multiple sensors can be embedded between multiple layers of sample and the in-situ monitoring can be carried out to investigate the differences in the exerted strain on different layers and at different positions along the sample.
- For profiling the strain distribution of a single layer of the sample, feasibility of using multiple multiplexed EFPI sensors can be explored due to their small size.
- Feasibility of reducing the length of the IFPI sensors further can be investigated. Reduction in the IFPI sensor length will result in reduction of the hybrid sensor length. Smaller size of the hybrid sensor will make it easier for embeddable applications, specifically for laboratory investigation of strain response of polymer materials since a desired dimension of testing samples limit these applications.
- Simplifying the signal extraction from the hybrid spectra can be investigated. Programming tools other than MATLAB can be investigated for faster processing.
- Effect of different combinations of post-cure temperature and time can be studied to see the changes in strain characteristics of the embedded samples.
- BMI is a new material and there are many opportunities to study different characteristics of the material that could provide more insight to its applications and limitations. FPI-based sensors can be used to study material characteristics beyond testing the temperature and strain limits.

APPENDIX A

STEPS INVOLVED IN MANUFACTURING BMI SAMPLES FOR EMBEDDED SENSOR TESTING

This appendix includes a step-by-step description of the process involved in manufacturing the BMI samples with embedded sensors. Pictures of each step are provided for better understanding of the process.

STEP 1: A thick Aluminum plate/mold is prepared by cleaning it with alcohol-based cleaner. Multiple layers of the BMI material lined with BMI resin are laid up on top of each other. These layers can be seen in black color in the picture below. The sensor to be embedded is placed in between the central layers of BMI. The sensor is placed right in the middle to avoid any edge effects and a shrinking tube is used at the egress point to avoid breaking the fiber by the hardening material. The sensor and the shrinking tubes can be seen held in place by blue tape. A double tape (resin dam) is placed around the sample to prevent the resin leaking out and affect any other samples on the mold. Metal meshes are placed around the sample for even application of applied pressure and a laminate sheet is used to cover the arrangement.

Figure A.1 BMI sample assembly with the optical fiber sensor before cure process.

STEP 2: Depending upon the size of the mold, multiple samples can be manufactured at the same time. The picture below shows two samples ready to be manufactured on the same mold.

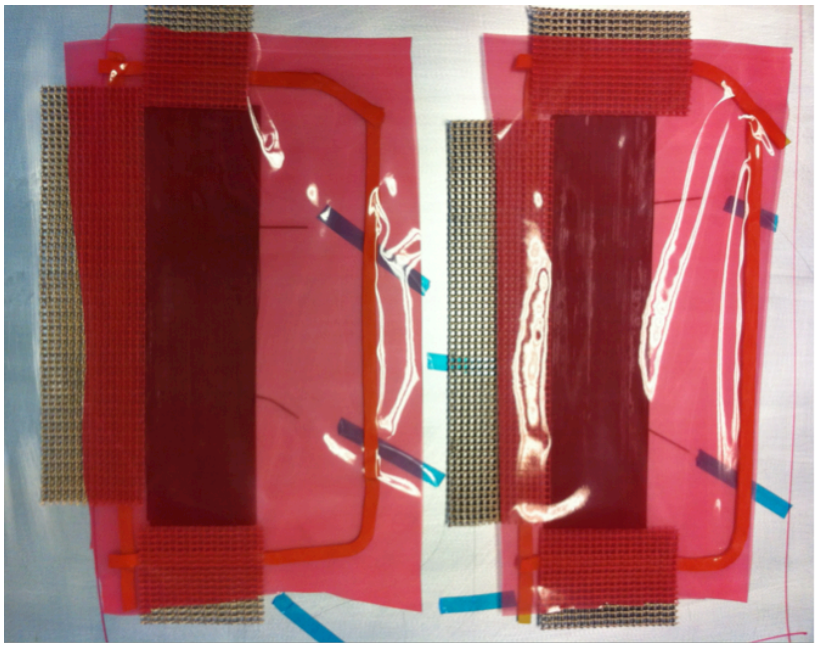

Figure A.2 Assembly for two samples to be prepared simultaneously.

STEP 3: A breather fabric is used to cover all the sample arrangements on the mold. A piece of metal mesh is placed marking the location of placement of the suction hose.

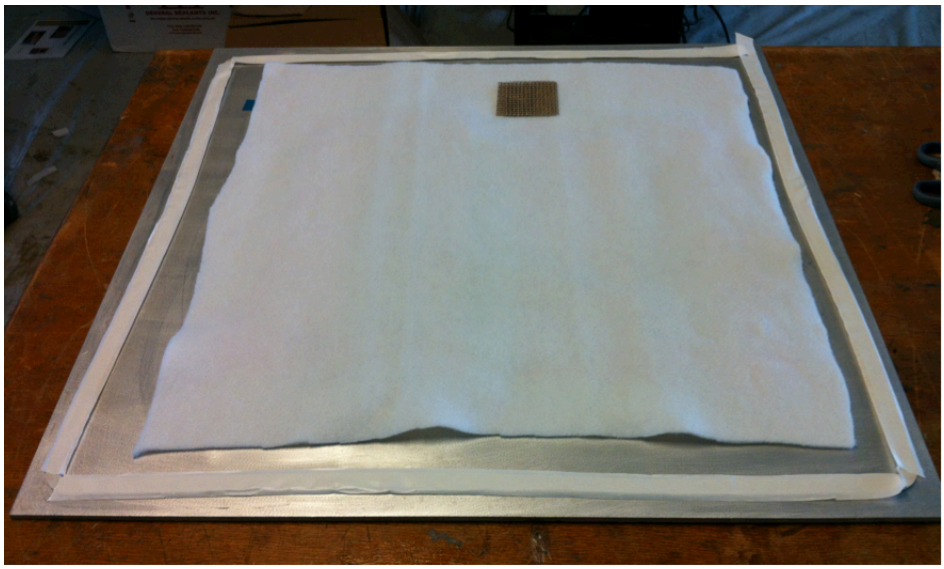

Figure A.3 Sample assembly covered with the breather fabric.

STEP 4: The whole arrangement is covered using another laminate sheet and suction is applied to maintain a full atmospheric pressure. The following picture is of the set up for manufacturing four samples simultaneously. The resin dams separating the samples can also be seen.

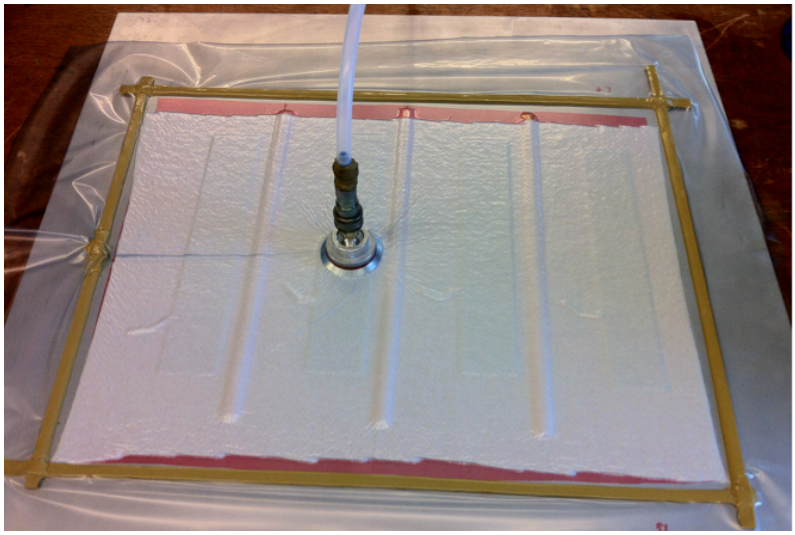

Figure A.4 Assembly attached to the vacuum pump.

STEP 5: The mold with the sample set up is kept inside a furnace for the curing process, the samples are under vacuum throughout the curing process. The following picture shows the vacuum pump attached to the mold.

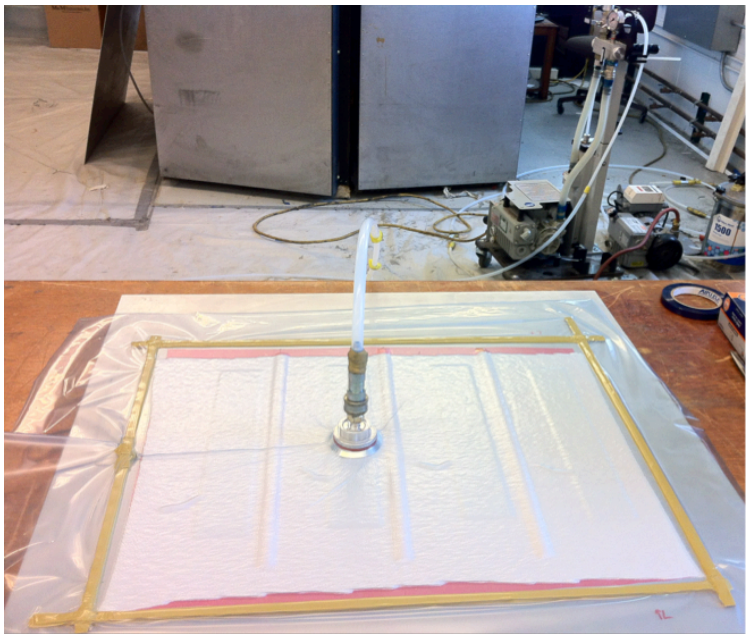

Figure A.5 Manufacturing set up before the mold was kept inside the oven.

STEP 6: The following picture shows the in-situ monitoring of the curing process being carried out using an optical spectrum analyzer while the mold with the BMI sample-set up is undergoing the curing process inside the furnace.

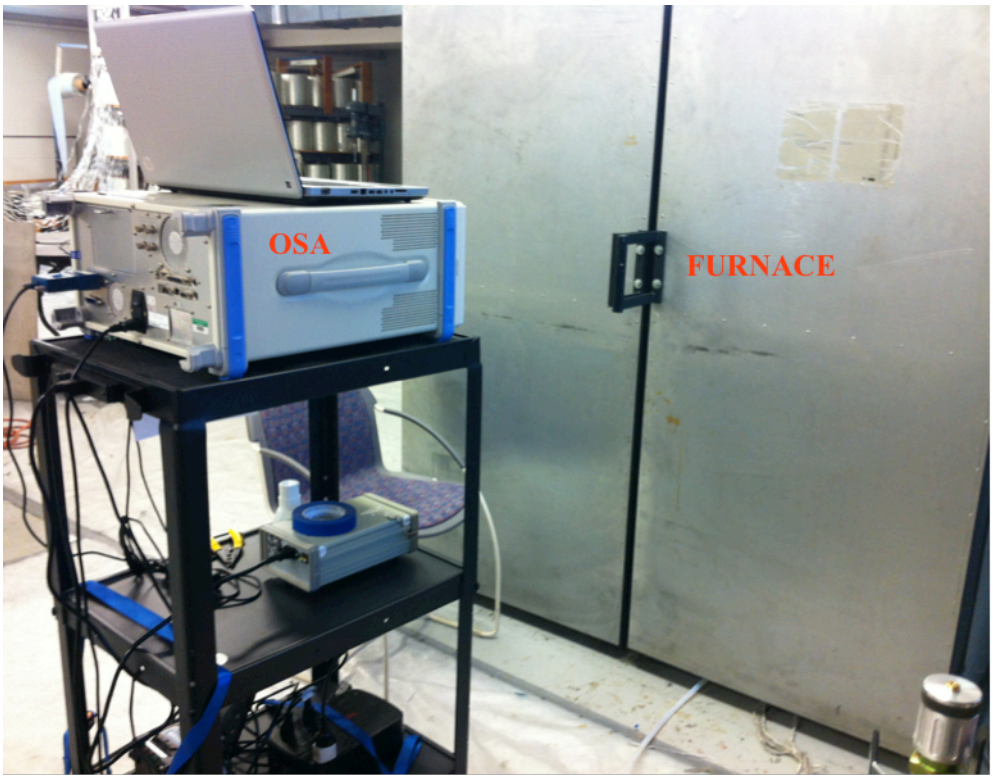

Figure A.6 In-situ monitoring of the cure process.

STEP 7: The last step is to let the sample cool down inside the closed furnace to complete the cure process. Once the cure process is complete, the breather fabric and other protective sheets are carefully removed and BMI samples with the embedded sensors are carefully lifted off the aluminum mold. Aluminum tabs are then fixed at both ends of these samples so that they can be held in place by the grips of the strain applicator INSTRON machine. These tabs prevent the sample from breaking due to the pressure applied by the grips before the actual strain loading starts. The following pictures show the top and bottom views of a sample with tabs affixed. The optical fiber can be seen coming out of a side of the sample.

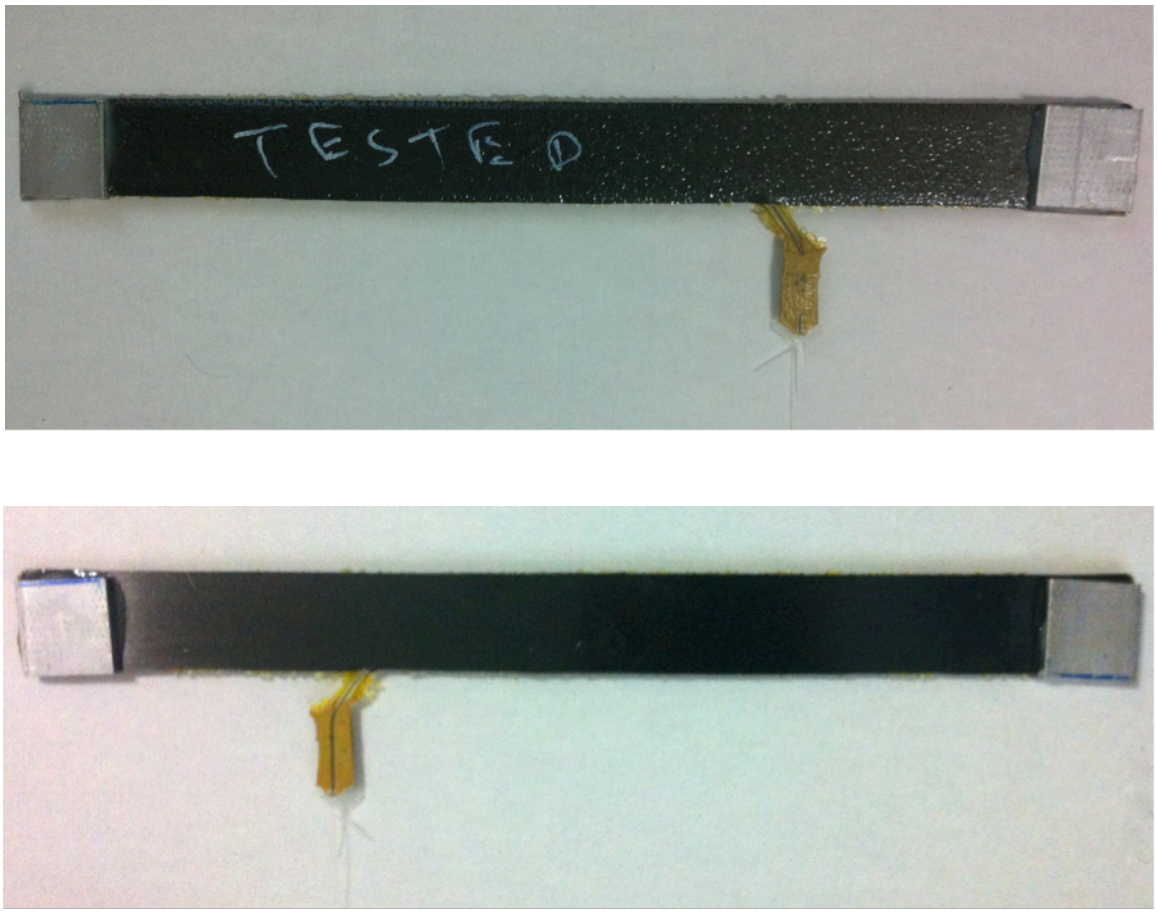

Figure A.7 Prepared BMI sample with aluminum tabs attached.

APPENDIX B

BMI EMBEDDED SENSOR TESTING

This appendix includes more pictorial information on embedded sensor testing, sample placement for the testing and failed sensors.

Sample placement for strain testing: The following picture shows the BMI sample placement between the INSTRON machine's strain frame grips. Also shown in the picture is the instrumentation set up used for in-situ monitoring of the embedded sensor response. The instrumentation includes a power source, optical spectrum analyzer and a computer unit equipped with data processing software (for the work presented in this dissertation, MATLAB was used).

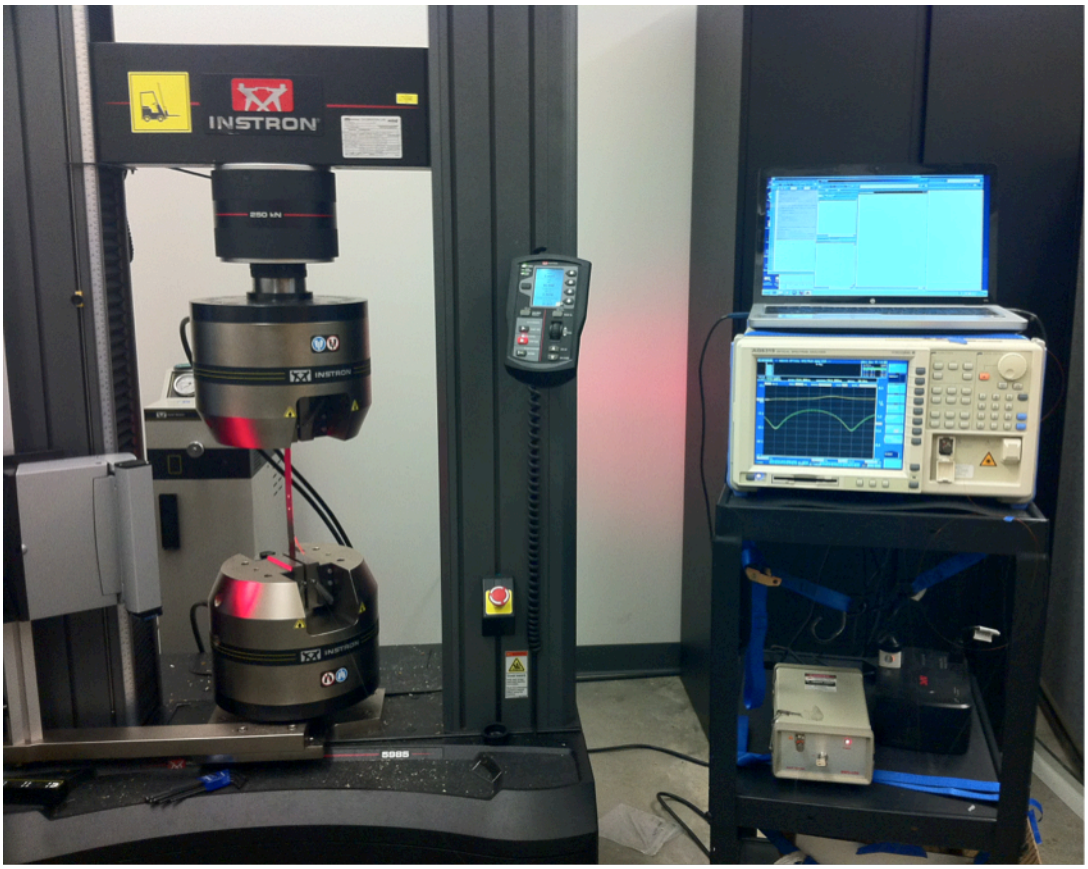

Figure B.1 Strain testing set up for the embedded sensors.

Sample Failure – Longitudinal Split: The following picture shows a longitudinal split as a result of the substrate failure at which point the sensor also broke. The split results due to a non-perfect alignment of the BMI laminate sheets.

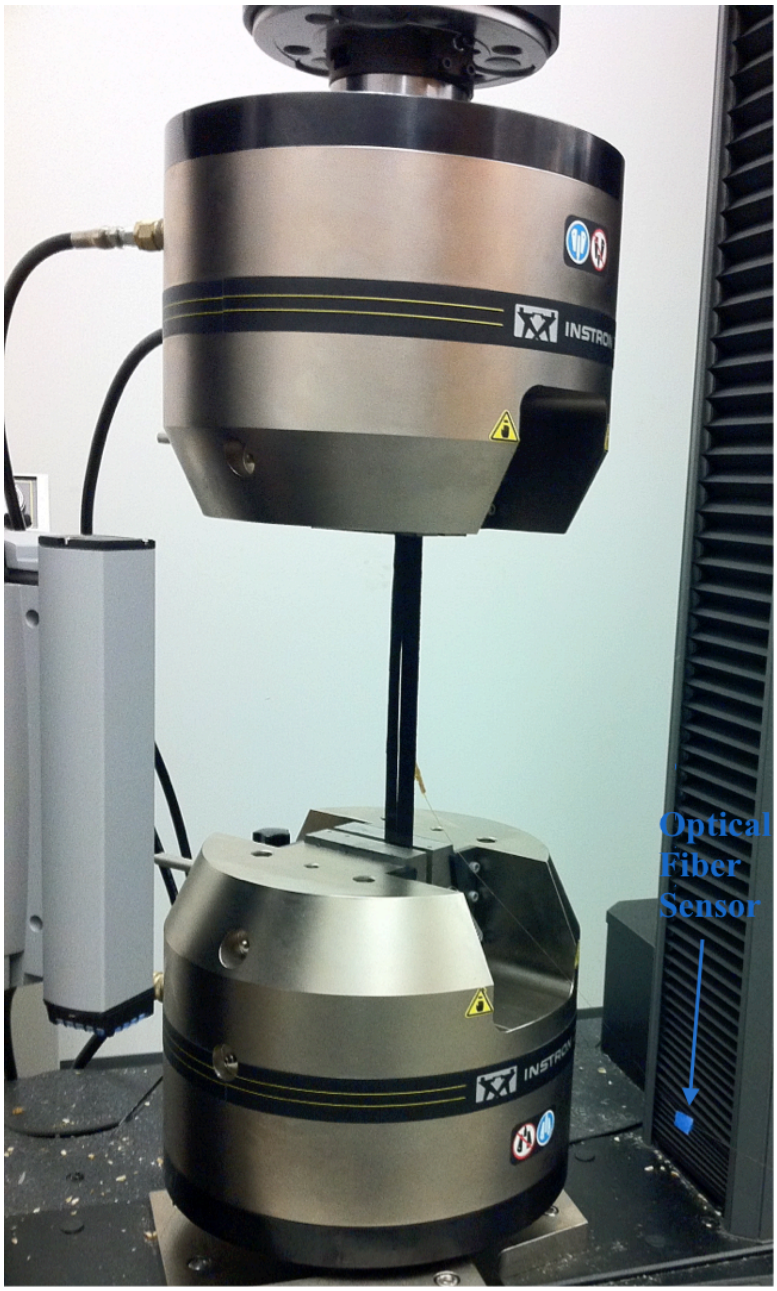

Figure B.2 Longitudinal split shown along the sample length.

Complete Sample Failure: The following picture shows a complete sample failure where the material could no longer bear the strain and splits at multiple points. As a result of the substrate failure, the sensor also broke.

Figure B.3 Complete sample failure due to large exerted strain.

The following is a close-up of a completely failed sample as a result of exerted strain outside of the materials' limits. Also, the aluminum tabs can be seen in the picture. These tabs are attached to the sample post curing process to avoid damaging the sample from exerted pressure by the strain application grips.

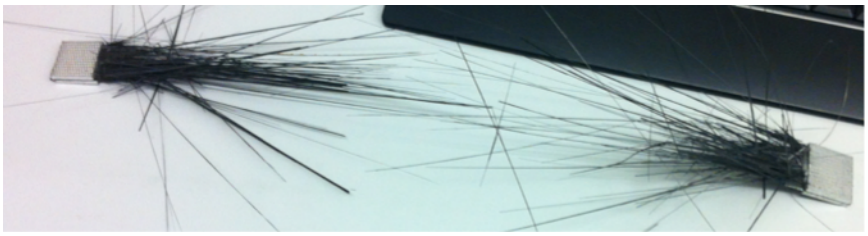

Figure B.4 Composite fibers can be seen after the sample failure.

BIBLIOGRAPHY

[1] E. Udd, "An Overview of Fiber-optic Sensors," *Review of Scientific Instruments*, vol. 66(8), pp 4015-4030, 1995.

[2] R. Kashyap, "Photosensitive Optical Fibers: Devices and Applications," *Optical Fiber Technology*, vol. 1(1), pp 17-34, 1994.

[3] R. M. Measures, "Advances Toward Fiber Optic Based Smart Structures," *Opt. Eng.*, vol. 31(1), pp 34-47, 1992.

[4] V. M. Murukeshan, P. Y. Chan, L. S. Ong, and L. K. Seah, "Cure monitoring of smart composites using Fiber Bragg Grating based embedded sensors," *Sensors and Actuators A: Physical*, vol. 79, pp 153-161, 2000.

[5] J. Etches, and G. Fernando, "Evaluation of Embedded Optical Fiber Sensors in Composites: EFPI Sensor Response to Fatigue Loading," *Polymer Composites*, vol. 31, pp 284-291, 2010.

[6] V. Zetterlind, S. Watkins, and M. Spoltman, "Fatigue Testing of a Composite Propeller Blade using Fiber Optic Strain Sensor," *Sensors Journal IEEE*, vol. 3 (4), pp 393-399, 2003.

[7] X. Jin, J. Chung, and V. Venkat, "Simultaneous Measurement of Two Strain Components in Composite Structures Using Embedded Fiber Sensor," *Journal of Composite Materials*, vol. 33 (15), pp 1376-1389, 1999.

[8] P. Choquet, F. Juneau, and F. Dadoun, "New Generation of Fiber-Optic Sensors for Dam Monitoring" *Proceedings of the 1999 International Conference on Dam Safety and Monitoring*, pp 19–22, 1999.

[9] V. Bhatia, M. Sen, K. Murphy, R. Claus, M. Jones, J. Grace, T. Tran, and J. Greene, "Optical Fiber Extrinsic Fabry-Perot Interferometeric Strain Sensor for Multiple Strain State Measurements," *SPIE*, vol. 2444, pp 115-126, 1995.

[10] Y. Rao, S. Yuan, X. Zeng, D. Lian, Y. Zhu, Y. Wang, S. Huang, T. Liu, G. Fernando, L. Zhang, and I. Bennion, "Simultaneous Strain and Temperature Measurement of Advanced 3-D Braided Composite Materials using an Improved EFPI/FBG system," *Optics and Lasers in Engineering*, vol. 38, pp 557-566, 2002.

[11] L. Matus, "Instrumentation for Aerospace Applications: Electronic-Based Technologies," *Journal of Aerospace Engineering*, vol. 26, pp 409-421, 2013.

[12] D.S. Eddy, and D. R. Sparks, "Applications of MEMS technology in Automotive Sensors and Actuators," *Proceedings of the IEEE*, vol. 86(8), pp 1747-1755, 1998.

[13] N. G. Wright, and A. B. Horsfall, "SiC sensors: A Review," *Journal of Physics D: Applied Physics*, vol. 40(20), 6345-6354, 2007.

[14] Y. Kanda, "Piezoresistance effect of silicon," *Sensors and Actuators A: Physical*, vol. 28, pp 83-91, 1991.

[15] J. Zhou, S. Dasgupta, H. Kobayashi, J. M. Wolff, H. E. Jackson, and J. T. Boyd, "Optically interrogated MEMS pressure sensors for propulsion applications," *Optical Engineering*, vol. 40, pp 598-604, 2001.

[16] F. Abu-Farha, M. Nazzal, O. Rawashdeh, and R. Michael, "Contact Sensors for Accurate Monitoring and Prediction of Sheet Deformation during Hydro/Pneumatic Forming Operations," *Key Engineering Materials*, vol. 433, pp 125-132, 2010.

[17] K. Zhou, M. Dubov, C. Mou, L. Zhang, V. K. Mezentsev, and I. Bennion, "Line-by-Line Fiber Bragg Grating Made by Femtoseond Laser," *IEEE Photonics Technology Letters*, vol. 22(16), pp 1190-1192, 2010.

[18] R. J. Williams, C. Voigtländer, G. D. Marshall, A. Tünnermann, S. Nolte, M. J. Steel, and M. J. Withford, "Point-by-point inscription of apodized fiber Bragg gratings," *Optics Letters*, vol. 36 (15), pp 2988-2990, 2011.

[19] J. Thomas, N. Jovanovic, R. G. Becker, G. D. Marshall, M. J. Withford, A. Tünnermann, S. Nolte, and M. J. Steel, "Cladding mode coupling in highly localized fiber Bragg gratings: modal properties and transmission spectra," *Optics Express*, vol. 19(1), pp 20651-20660, 2011.

[20] M. N. Ng, and K. S. Chiang, "Thermal effects on the transmission spectra of long-period fiber gratings," *Optics Communications*, vol. 208 (4), pp 321-327, 2008.

[21] A. M. Vengsarkar, P. J. Lemaire, J. B. Judkins, V. Bhatia, T. Erdogan, and J. E. Sipe, "Long-period fiber gratings as band-rejection filters," *Journal of Lightwave Technology*, vol.14, pp 58-64, 1996.

[22] J. Wang, and J. Tang, "Feasibility of Fiber Bragg Grating and Long-Period Fiber Gratins Sensors under Different Environmental Conditions," *Sensors*, vol. 10(11), pp 10105-10127, 2010.

[23] Y. W. Hu, X. Y. Sun, J. A. Duan, P. Lio, and X. N. Zhu, "The Effect of Refractive Index Modification Position and Duty Cycle on Performance of LPFGs," *IEEE Symposium on Photonics and Optoelectronics*, pp 26-28, 2011.

[24] B. H. Lee, Y. H. Kim, K. S. Park, J. B. Eom, M. J. Kim, B. S. Rho, and H. Y. Choi, "Interferometric Fiber Optic Sensors," *Sensors*, vol. 12(3), pp 2467-2486, 2012.

[25] V. R. Machavaram, R. A. Badcock, and G. Fernando, "Fabrication of intrinsic fiber Fabry-Perot sensors in silica fibers using hydrofluoric acid etching," *Sensors and Actuators A: Physical*, vol. 138(1), pp 248-260, 2007.

[26] D. Wu, T. Zhu, G. Wang, J. Fu, X. Lin, and G. Gou, "Intrinsic fiber-optic Fabry-Perot interferometer based on arc discharge and single-mode fiber," *Applied Optics*, vol. 52(12), pp 2670-2675, 2013.

[27] D. Jáuregui-Vázquez, J. M. Estudillo-Ayala, R. Rojas-Laguna, E. Vargas-Rodríguez, J. M. Sierra-Hernández, J. C. Hernández-Garcia, and R. I. Mata-Chávez, "An All Fiber Intrinsic Fabry-Perot Interferometer Based on an Air-Microcavity," *Sensors*, vol. 13(5), pp 6355-6364, 2013.

[28] T. Yoshino, K. Kurasawa, and I. Katsuji, "Fiber-Optic Fabry-Perot Interferometer and its Sensor Applications," *IEEE J. Quantum Electronics* 10, pp 1624-1633, 1982.

[29] A. D. Kersey, D. A. Jackson, and M. Corke, "A Simple Fiber Fabry-Perot Sensor," *Opt. Communication,* vol. 45, pp 71-74, 1983.

[30] D. Hogg, D. Janzen, T. Valis, and R. M. Measures, "Development of a Fiber Fabry-Perot Strain Gauge," *Proc. SPIE,* vol. 1588, pp 300-307, 1991.

[31] W. Zhao, J. Wang, A. Wang, and R. O. Claus, "Geometric Analysis of Optical Fiber EFPI Sensor Performance," *Smart Materials and Structures,* vol. 7(6), pp 907-910, 1998.

[32] J. Sirkis, T. A. Berkoff, R. T. Jones, H. Singh, A. D. Kersey, E. J. Friebele, and M. A. Putnam, "In-Line Fiber Etalon (ILFE) Fiber-optic Strain Sensors," *Journal of Lightwave Technology*, vol. 13(7), pp 1256–1263, 1995.

[33] J. Villatoro, V. Finazzi, G. Coviello, and V. Pruneri, "Photonic-crystal-fiber-enabled Micro-Fabry-Perot Interferometer," *Optics Letters*, vol. 34(16), pp 2441–2443, 2009.

[34] F. C. Favero, G. Bouwmans, V. Finazzi, J. Villatoro, and V. Pruneri, "Fabry-Perot Interferometers Built by Photonic Crystal Fiber Pressurization during Fusion Splicing," *Optics Letters*, vol. 36(21), pp 4191–4193, 2011.

[35] F.C. Favero, L. Araujo, G. Bouwmans, V. Finazzi, J. Villatoro, and V. Pruneri, "Spheroidal Fabry-Perot Microcavities in Optical Fibers for High-sensitivity Sensing," *Optics Express*, vol. 20(7), pp 7112-7118, 2012.

[36] Y. J. Rao, M. Deng, D. W. Duan, X. C. Yang, T. Zhu, and G. H. Cheng, "Micro Fabry-Perot interferometers in silica fibers machined by femtosecond laser," *Optics Express*, vol. 15(21), 14123–14128 (2007).

[37] E. Cibula, S. Pevec, B. Lenardili, É. Pinet, and D. Onlagi, "Miniature All-glass Robust Pressure Sensor," *Optics Express*, vol. 17(7), pp 5098-5106, 2009.

[38] A. Kaur, S. Nagarajan, S. Anandan, L. Yuan, K. Chandrashekhara, S. E. Watkins, and N. Pham, "Embeddable Fiber Optic Strain Sensor for Structural Monitoring," *SPIE Proceedings*, vol. 8692, 86921W, 2013.

[39] V. M. Murukeshan, P. Y. Chan, L. S. Ong, and L. K. Seah, "Cure monitoring of smart composites using Fiber Bragg Grating based embedded sensors," *Sensors and Actuators A: Physical*, vol. 79, pp 153-161, 2000.

[40] J. Etches, and G. Fernando, "Evaluation of Embedded Optical Fiber Sensors in Composites: EFPI Sensor Response to Fatigue Loading," *Polymer Composites*, vol. 31, pp 284-291, 2010.

[41] X. Jin, J. Chung, and V. Venkat, "Simultaneous Measurement of Two Strain Components in Composite Structures Using Embedded Fiber Sensor," *Journal of Composite Materials*, vol. 33 (15), pp 1376-1389, 1999.

[42] J. Nelson, A. Hine, P. Segdwick, R. Lowe, E. Rexeisen, R. King, and N. Patz, "Development of Nano-Silica Bismalimide (BMI) Matrix Resins for Prepeg Tooling Composites: Fortified Tooling Prepeg BMI," *SAMPE Technical Conference*, Baltimore MD, pp 1-13, 2013.

[43] S. Anandan, S. Nagarajan, A. Kaur, K. Chandrashekhara, H. Xiao, and N. Phan, "Monitoring of Out-of-Autoclave BMI Composites using Fiber Optic Sensors," *Proceeding of SPIE*, vol. 8694, pp M1 – M6, 2013.

[44] S. E. U. Lima, O. Frazão, R. G. Farias, F. M. Araújo, L. A. Ferreira, V. Miranda, and J. L. Santos, "Intrinsic and extrinsic fiber Fabry-Perot sensors for acoustic detection in liquids," *Microwave and Optical Technology Letters*, vol. 52(5), pp 1129-1134, 2010.

[45] C. Ma, and A. Wang, "Multimode excitation-induced phase shifts in intrinsic Fabry-Perot interferometric fiber sensor spectra," *Applied Optics*, vol. 49(25), pp 4836-4845, 2010.

[46] N. Jovanovic, J. Thomas, R. William, M. J. Steel, G. D.Marshall, F. Alexander, S. Nolte, A. Tünnermann, M. J. Withford, "Polarization-dependent effects in point-by-point fiber Bragg gratings enable simple, linearly polarized fiber lasers," *Optics Express*, vol. 17(8), pp 6082-6095, 2009.

[47] M. Born, and E. Wolf, *Principles of Optics*, 6th (corrected) ed., Pergamon Press, Oxford, U.K., 1980.

[48] S. H. Aref, H. Latifi, M. I. Zibaii, and M. Afshari, "Fiber optic Fabry-Perot pressure sensor with low sensitivity to temperature changes for downhole application," *Optics Communications*, vol. 269, pp 322-330, 2007.

[49] K. Bremer, E. Lewis, G. Leen, B. Moss, S. Lochmann, and I. A. R. Mueller, "Feedback Stabilized Interrogation Technique for EFPI/FBG Hybrid Fiber-Optic Pressure and Temperature Sensors," *IEEE Sensors Journal,* vol. 12(1), pp 133-138, 2012.

[50] Available: http://accuratus.com/fused.html, July 28, 2014.

[51] P. P. Parlevliet, H. E. N. Bersee and A. Beukers, "Shrinkage determination of a reactive polymer with volumetric dilatometry," *Polymer Testing*, vol. 29(4), pp 433-439, 2010.

[52] Y. Nawab, X. Tardif, N. Boyard, V. Sobotka, P. Casari and F. Jacquemin, "Determination and modeling of the cure shrinkage of epoxy vinylester resin and associated composites by considering thermal gradients," *Composites Science and Technology*, vol. 73, pp 81-87, 2012.

[53] Y. Han, and S. B. Lee, “Simultaneous measurement of temperature and strain using dual long-period fiber gratings with controlled temperature and strain sensitivities,” *Optics Express*, vol. 11(5), pp 476-481, 2003.

[54] J. -L. Tang, and J. –N. Wang, “Error analysis and measurement uncertainty for a fiber grating strain-temperature sensor,” *Sensors*, vol. 10, pp 6582-6593, 2010.

[55] D. –P. Zhou, L. Wei, W. – K. Liu, and J.Lit, “Simultaneous Temperature and Strain Measurement Using Fiber Bragg Gratings and Multi-Mode Fiber,” *IEEE Photonics Letters*, vol. 21(7), pp 468-470, 2009.

[56] M. J. Kim, Y. H. Kim, and B. H. Lee, “Simultaneous measurement of temperature and strain based on double cladding fiber interferometer assisted by fiber grating pair,” *IEEE Photonics Technology Letters*, vol. 20, pp 1290-1292, 2008.

[57] Y. Zhang, J. Huang, X. Lan, L. Yuan, and H. Xiao, “Simultaneous measurement of temperature and pressure with cascaded extrinsic Fabry-Perot interferometer and intrinsic Fabry-Perot interferometer sensors,” *Optical Engineering*, vol. 53(6), 067101, 2014.

[58] W. Wang, J. Wen, F. Pang, N. Chen, and T. Wang, "All single mode fiber Fabry-Perot interferometric high temperature fabricated with femtosecond laser," *Chinese Journal Lasers*, vol. 39, pp. 1005001, 2012.

[59] W. Wang, D. Ding, N. Chen, and F. Pang, "Quasi-Distributed IFPI Sensing System Demultiplexed With FFT-Based Wavelength Tracking Method," *IEEE Sensors Journal*, vol. 12, pp. 2875-2880, 2012.

VITA

Amardeep Kaur was born in Gondpur Hoshiarpur (Punjab), India. She completed her Bachelor of Technology in Electronics and Communication Engineering at Punjab Technical University in Punjab, India in May 2006. In August 2007, Amardeep joined the Department of Electrical and Computer Engineering at Missouri University of Science and Technology to pursue a masters' degree under the guidance of Dr. Steve E. Watkins. She received her Master of Science degree in 2009.

With a penchant in Electrical Engineering and liking to know more about her field, Amardeep continued studying towards a doctoral degree under the guidance of Drs. Hai Xiao and Steve E. Watkins. Focus of her research was to develop and demonstrate novel strain and temperature sensors for structural health monitoring. In December 2014, she received her Ph.D. in Electrical Engineering from Missouri University of Science and Technology. During her graduate study, she authored and co-authored 8 journal papers and 3 conference papers and reviewed several papers for Chinese Optics Letters. While at Missouri S&T, Amardeep served as the Secretary and then, the Vice-President of the Council of Graduate Students (the graduate students' governing body). She also served on the International Student Advisory Board.